BIOCHEMISTRY
including biophysical chemistry & molecular biology

Article

pubs.acs.org/biochemistry

Experimental and Computational Investigations of Oxygen Reactivity in a Heme and Tyrosyl Radical-Containing Fatty Acid α-(Di)oxygenase

Gregory S. Huff,[†] Irina S. Doncheva,[†] David W. Brinkley,[†] Alfredo M. Angeles-Boza,[†] Arnab Mukherjee,[†] Christopher J. Cramer,*[,‡] and Justine P. Roth*[,†]

[†]Department of Chemistry, Johns Hopkins University, 3400 North Charles Street Baltimore, Maryland 21218, United States

[‡]Department of Chemistry and Supercomputing Institute, University of Minnesota, 207 Pleasant St. SE, Minneapolis, Minnesota 55455, United States

Supporting Information

ABSTRACT: Rice α-(di)oxygenase mediates the regio- and stereospecific oxidation of fatty acids using a persistent catalytic tyrosyl radical. Experiments conducted in the physiological O_2 concentration range, where initial hydrogen atom abstraction from the fatty acid occurs in a kinetically reversible manner, are described. Our findings indicate that O_2-trapping of an α-carbon radical is likely to reversibly precede reduction of a 2-(*R*)-peroxyl radical intermediate in the first irreversible step. A mechanism of concerted proton-coupled electron transfer is proposed on the basis of natural abundance oxygen-18 kinetic isotope effects, deuterium kinetic isotope effects, and calculations at the density functional level of theory, which predict a polarized transition state in which electron transfer is advanced to a greater extent than proton transfer. The approach outlined should be useful for identifying mechanisms of concerted proton-coupled electron transfer in a variety of oxygen-utilizing enzymes.

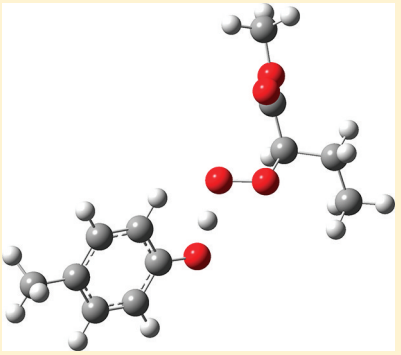

Rice fatty acid α-(di)oxygenase (RαO) is a member of the pathogen-inducible oxygenase (PIOX)[2] family of membrane-associated heme proteins.[3] As such, it is recruited to produce oxylipins[4,5] that function in cell signaling, wound healing, and the protection of plants from infection.[6−11] The proteins are also recognized for their structural homology[1,12−14] to the mammalian cyclooxygenases (COX-1 and COX-2),[15,16] which utilize a Tyr• to oxidize arachidonic acid in the first committed step of prostaglandin biosynthesis. The detailed mechanisms of such fatty acid oxidations remain incompletely understood, especially with regard to the coupling of proton and electron transfer steps during the formation of various radical intermediates. These events are critical to understand because they control the activation and deactivation of enzymes implicated in oxidative stress.

RαO contains a conserved Tyr• that has been proposed to effect the insertion of O_2 into the $C_α$−H bonds, adjacent to the carboxylate group, in saturated and unsaturated fatty acids.[17,18] Upon release from the enzyme, the 2-*R*-hydroperoxide product undergoes spontaneous decarboxylation to form a linear aldehyde.[1] Although RαO has not been crystallographically characterized,[19] homology modeling predicts the active site depicted in Figure 1, where the conserved Tyr379 resides ∼6 Å away from the Fe^{III} protoporphyrin IX (Por) and <4 Å away from His311.[17,20] Another pairing of His and Tyr is observed in photosystem II, where the catalytic Tyr• is generated

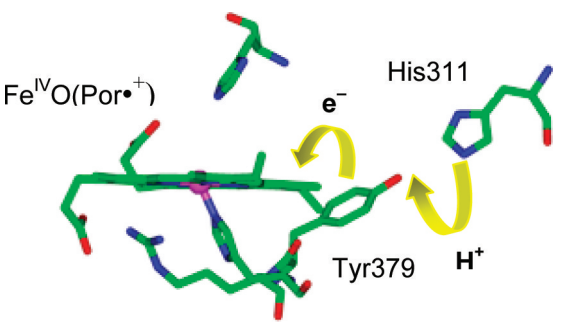

Figure 1. Homology model depicting a proton-coupled electron transfer pathway in RαO.

photochemically by a mechanism which is believed to involve electron transfer prior to proton transfer.[21,22] In general, it is difficult to determine how proton and electron motions are coupled due to the absence of suitable isotopic probes.

Multiple proton-coupled electron transfer (PCET) steps are involved in the catalytic cycle of RαO, providing a fruitful testing ground for how protein structures discourage the formation of high-energy intermediates and facilitate lowering

Received: July 1, 2011
Revised: July 18, 2011
Published: July 26, 2011

of as well as tunneling through thermal activation barriers. In the initiating step, Tyr379 donates an electron to the oxidized prosthetic group, either Fe^{IV}=O($Por^{\bullet+}$) or Fe^{IV}=O(Por), prior to proton transfer to a nearby base, possibly His311.[17,18] It is not known whether this reaction occurs by concerted or sequential PCET. In fact, there is very little precedent for concerted PCET in redox enzymes in general.[23] RαO contains two other His residues proximal and distal to the prosthetic group. Such structures are typically found in peroxidase enzymes;[24] however, RαO exhibits no such activity.[18,25] Instead, the enzyme catalyzes H_2O_2 disproportionation, in a manner that protects the protein from autoxidation.

The stability of the Tyr379$^{\bullet}$ in RαO has allowed for its characterization by electron paramagnetic resonance (EPR) spectroscopy at ambient temperature as well as in frozen solutions.[17,18] Treatment with H_2O_2 amplifies the Tyr379$^{\bullet}$-associated EPR signal, which is reduced by many fatty acid substrates with the exception of those lacking C_α−H bonds.[17] An increase in α-dioxygenase activity is also detectable upon addition of substoichiometric H_2O_2 equivalents. Under these conditions, Fe^{III}(Por) accumulates because of the slow rate of forming Fe^{IV}O($Por^{\bullet+}$) and Fe^{IV}O(Por) relative to their more rapid rates of reduction. As a result, it is not known which of the ferryl species directly oxidizes Tyr379. A reducing equivalent remains unidentified and only 25−30% of the unpaired spin can be accounted for after decay of the primary Fe^{IV}O($Por^{\bullet+}$) intermediate to Fe^{III}(Por).[17,18] The Tyr379Phe mutant also undergoes prosthetic group oxidation, albeit much slower, while acting as a H_2O_2 disproportionation catalyst. No persistent EPR signal nor α-dioxygenase activity is detected in the mutant, implicating Tyr379$^{\bullet}$ as the active catalyst.[17,18]

C_α−H bond oxidation by the Tyr379$^{\bullet}$ in RαO has recently been examined at pH 7.2 and 22 °C with hexadecanoic (16:0), dodecanoic (12:0), and decanoic (10:0) acids or fatty acids (FAs).[18] Kinetic studies expose apparent second-order rate constants, $^{ap}k_{cat}/K_M$(FA) and $^{ap}k_{cat}/K_M(O_2)$, which depend upon the concentration of the corresponding cosubstrate; these values exhibit a hyperbolic increase to limiting values of k_{cat}/K_M(FA) and $k_{cat}/K_M(O_2)$. These results, together with the hyperbolic increase in the deuterium kinetic isotope effects (KIEs) on fatty acid oxidation to $^{D}k_{cat}/K_M$(FA) at saturating O_2 concentration, are uniquely consistent with the mechanism in Scheme 1, where it is predicted that Tyr379$^{\bullet}$-mediated hydrogen atom transfer transitions from irreversible to reversible upon lowering the concentration of O_2. In the low O_2 limit, the turnover rate constant is determined by reversible O_2-trapping of the α-carbon radical in a suprafacial manner followed by reduction of the 2-*R*-peroxyl radical intermediate.

This study utilizes DFT calculations to understand how RαO directs the reactivity of O_2 in the physiological concentration range (<50 μM).[26] Under these conditions, PCET determines the regio- and stereochemical fidelity of the products formed, while preventing accumulation of damaging oxygen radical intermediates. Although such reactions occur widely in nature,[26,27] little is known about the factors that dictate barrier heights and the accompanying electron/proton transfer probabilities. The combined experimental and computational approach featured in this study illuminates the reactivity of a tyrosyl radical utilizing dioxygenase through the analysis of competitive oxygen-18 KIEs, together with primary deuterium KIEs. As demonstrated for the first time, high-level density functional theory (DFT) calculations reproduce ^{18}O KIEs while providing insight as to the mechanism and transition state for PCET.[28]

EXPERIMENTAL SECTION

General. Chemical and biochemical reagents used in this study were obtained commercially in the highest purity available and used as received. The procedures for spectroscopic and kinetic characterization of RαO have been described earlier.[17,18] A brief summary of how ^{18}O KIEs are determined from natural abundance O_2 is presented below.

Protein Preparation. Following published procedures,[1,17,18] wild-type (wt) RαO was overexpressed as an N-terminal His_6-tagged homodimeric protein with a molecular weight of 145 kDa and a tightly bound Fe^{III}(Por). Preparations were of >98% purity, as indicated by polyacrylamide gel electrophoresis and amino acid analysis at the Texas A&M University sequencing center. The protein's structural integrity was confirmed by circular dichroism measurements on a Jasco J-810 polarimeter between pH 7.2 and 10.0 as well as at temperatures from 5 to 40 °C.[a]

Holoprotein Stock Solutions. Concentrations of RαO were determined from the optical absorption spectrum

Scheme 1. Free Energy Diagram for RαO Catalysis (Solid Curve); Effect of Increasing the O_2 Concentration to Saturating Levels, i.e. ~1 mM (Dashed Curve)

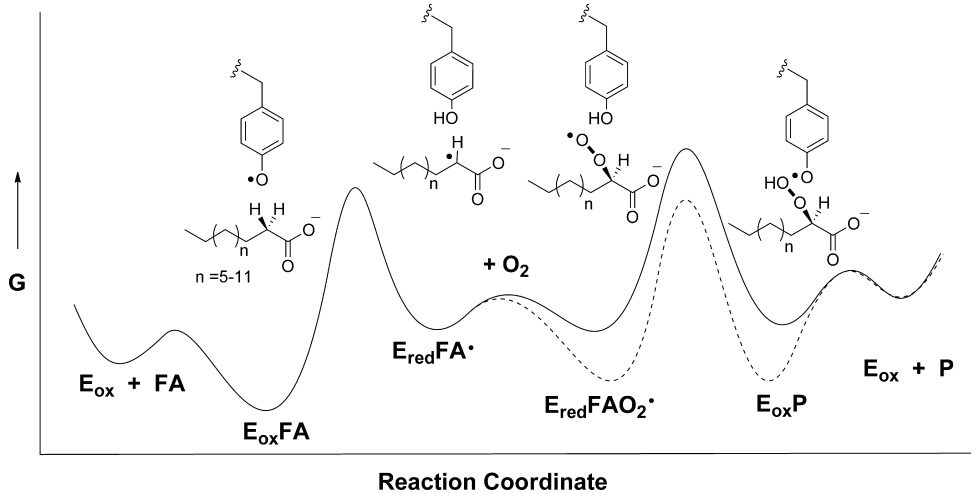

recorded on an Agilent 8453 diode array spectrophotometer. The characteristic Soret band of the Fe^{III}(Por) was observed together with distinctive Q-bands in the 500−600 nm region.[17] The molar extinction coefficient of the Soret band, $\varepsilon_{412\ nm}$ = 123 000 M^{-1} cm^{-1}, was determined by the pyridine hemochrome assays under oxidizing and reducing conditions.[29] A standard assay was then developed assuming one Tyr379$^{\bullet}$ per equivalent of Fe^{III}(Por). This standard assay was undertaken at pH 7.2 in air-saturated solutions containing h_{31}-16:0 (50−100 μM) and O_2 (~272 μM) to determine $V/[E]$ = 9.0 s^{-1} at 22 ± 0.2 °C.[18] A YSI Clark-type electrode was employed for measurements of O_2 consumption rates.

Consistent with earlier EPR spectroscopic studies using an X-band Bruker EMX spectrometer, wt-RαO exhibited a multiline signal centered at g = 2.0054, which was absent in the Tyr379Phe mutant.[17] The distinctive radical signature, generated upon addition of H_2O_2 to wt-RαO, persists for minutes at ambient temperature. The radical is also detectable at lower concentrations in freshly isolated protein solutions. Enzyme turnover can, therefore, be achieved without the addition of H_2O_2, which amplifies the EPR signal as well as the α-dioxygenase activity without affecting the steady-state kinetic parameters.

Steady-State Kinetics. Initial rates at variable O_2 concentrations were determined at pH 7.2 and 22.0 ± 0.2 °C unless noted otherwise. Reactions initiated by introducing the enzyme or the fatty acid, dissolved in ethanol, gave essentially the same results. When H_2O_2 was added to optimize enzyme activity, care was taken to ensure that O_2 evolution due to the catalytic H_2O_2 disproportionation had ceased before recording the rates. In general, a correction for the background drift of the O_2 electrode was applied when it exceeded 5% of the initial rate.

Analysis of the kinetics using Kaleidagraph 4.0 (Synergy software) was routinely performed by fitting initial rate data to the Michaelis−Menten expression. In some cases, linear regression was used to fit the data at very low concentrations, i.e., less than one-half the $K_M(O_2)$.[30] Apparent rate constants, determined at subsaturating concentrations of O_2 or fatty acid, were fitted to hyperbolic expressions to obtain the limiting rate constants: k_{cat}, k_{cat}/K_M(FA), and $k_{cat}/K_M(O_2)$ ± 2 standard errors.

Viscosity Effects. Relative solution viscosities (η^{rel}) were measured using an Ostwald viscometer and referenced to a buffer-only solution (η^0) at 22 ± 2 °C. Increasing solution viscosity slows rates of diffusion-limited processes in a manner predicted by the Stokes−Einstein relation: $[k_{cat}/K_M(O_2)^0/k_{cat}/K_M(O_2)] = (\eta^{rel}/\eta^0)^{exp}$, where "0" designates the absence of added viscosogen and an exponent of 1 corresponds to a diffusion-limited process.[31] An empirically derived exponent of ~0.5 has been suggested for reactions of O_2 because of deviations from Stokes−Einstein behavior.[31−34] Viscosity experiments, therefore, employed solutions with high η^{rel} values. Control experiments were conducted using micro- and macro-viscosogens, glycerol, and Ficoll 400, respectively, in order to detect nonspecific effects arising from protein structural perturbation.

Solvent Kinetic Isotope Effects. The following buffers were used to test for solvent deuterium KIEs upon $k_{cat}/K_M(O_2)$ at an ionic strength of μ = 0.1 M: 0.0566 M sodium phosphate at pH 7.2 and 0.0107 M sodium pyrophosphate at pH 10. Deuterated buffers were prepared from D_2O and deuterium-enriched salts in an analogous manner. The pH and the pD of solutions were determined at 22 °C using an Accumet pH meter and the relation: $pH_{reading}$ = pD − 0.4.[35]

Deuterium Kinetic Isotope Effects. Substrate deuterium KIEs upon $k_{cat}/K_M(O_2)$, designated $^Dk_{cat}/K_M(O_2)$, were measured noncompetitively with the isotopically pure forms of the fatty acids. Earlier studies[18] demonstrated the retention of a single hydrogen from the α-position of the fatty acid by Tyr379$^{\bullet}$, which after reduction does not undergo detectable exchange with the solvent on the time scale of catalysis. The α-hydrogen from the fatty acid was, therefore, used to generate Tyr379(O−H) or Tyr379(O−D) for the determination of $^Dk_{cat}/K_M(O_2)$. To minimize systematic errors, multiple trials were performed using different sources of enzyme and fatty acids. The aggregate data from multiple researchers were averaged and are reported with propagated ±2 standard errors.

Measurement of Oxygen-18 Kinetic Isotope Effects. Competitive ^{18}O KIEs reflect the ratio of second-order rate constants corresponding to $k_{cat}/K_M(^{16,16}O_2)$ and $k_{cat}/K_M(^{16,18}O_2)$ at natural abundance levels. Samples of O_2 were collected using a specialized vacuum apparatus and published methodology[36,37]—described here briefly. Fatty acid solutions, saturated with O_2 or O_2/He, were sampled, and the pressure of O_2 and its isotope content was determined before and after introducing RαO. Each procedure required entraining the O_2 in a helium carrier gas so that it could be purified of all condensable gases, especially CO_2, by passage through a series of cold traps. The O_2 was then isolated on 5 Å molecular sieves at −196 °C. Following the removal of He, the O_2 was combusted quantitatively to CO_2.[36,37] As a result of combustion proceeding to 100% completion, the pressure and isotopic content of the CO_2 are identical to the O_2 from which it was formed. The CO_2 samples were condensed into dry glass tubes and flame-sealed for later analysis by dual-inlet isotope ratio mass spectrometry (IRMS) at the University of Waterloo, Environmental Isotope Laboratory.

Multiple trials were performed to determine the ^{18}O KIEs from the $^{18}O/^{16}O$ of the unreacted O_2 at time 0 (R_0) and the $^{18}O/^{16}O$ of the O_2 remaining (R_f) after some fractional conversion (f). Typically, the desired O_2 consumption was achieved by controlling the amount of fatty acid in the reaction solutions. As in the kinetics experiments, multiple sources of RαO and fatty acids were employed. The ^{18}O KIEs, analyzed numerically by solving eq 1, are quoted as the average of at least seven independent trials with errors of ±1 standard deviation about the mean. Isotope fractionation plots of the data fitted to eq 1 are used to illustrate the quality of the results.

$$^{18}O\ KIE = \left[1 + \frac{\ln(R_f/R_0)}{\ln(1-f)}\right]^{-1} \quad (1)$$

Density Functional Theory (DFT) Calculations. Enzymatically relevant processes were modeled using the reduced and oxidized forms of 4-methylphenol and methyl butanoate (i.e., the carboxylate ester of the four carbon fatty acid). Results with the deprotonated form of the parent fatty acid, butanoate, indicated that the negative charge on the carboxylate group led to optimized geometries with internal hydrogen bonding. This interaction within the 2-hydroperoxide structure transforms a pure O−H(D) stretching mode into lower frequency combination modes. The result is unlikely to be representative of

an actual conformation in the enzyme where active site residues and/or solvent molecules stabilize the carboxylate charge.

All molecular structures were optimized, either fully or subject to certain key distance constraints, at the density functional level of theory (DFT).[38] Using the Gaussian09 electronic structure suite,[b] the local generalized-gradient approximation (GGA) *m*PW functional[39−41] was employed together with the 6-311+G(2df,p) basis set for all atoms.[42] Vibrational frequencies were computed for the optimized structures and used to establish the nature of all stationary points along the reaction coordinate.

The vibrational frequencies determined for the ground-state structures were essentially indistinguishable from those calculated using *m*PW with a reduced basis set, namely 6-311G*(O), 6-31G (C), and STO-3G or 6-31G (H).[b] The trends in isotopic frequencies for the *m*PW calculations were also in reasonable agreement with those computed using the hybrid GGA B3LYP functional, but resorting to the B3LYP functional was not otherwise contemplated because it overestimates the O−O stretching frequency of O_2 as well as the isotope shift upon substituting ^{16}O with ^{18}O.

Calculations representative of the gas phase are used as a frame of reference in this study to assess the impact of a polarized enzyme active site. Electrostatic microenvironments within proteins have been proposed to cause catalytic rate accelerations in enzymes that react with O_2 by outer-sphere electron transfer.[43,44] Structural optimization and full vibrational frequency analyses were computed in the gas phase and with an aqueous dielectric continuum characterized by $\varepsilon_s = 78.3$ at 22 °C.[45,46] These limits were chosen, not because enzyme active sites are expected to be characterized by so low or high a dielectric constant, but rather to assess the effects at the two extremes. The aqueous SMD solvation model was used at the *m*PW/6-311+G(2df,p) level.[47−49] Although the active site of R*α*O is believed to be buried within the protein,[17−20] calculations undertaken with and without a dielectric continuum model offer insights as to how local polarization impacts the energetics and the ^{18}O isotope effects.[50]

Calculations of Oxygen-18 Isotope Effects. Oxygen-18 equilibrium isotope effects (^{18}O EIEs) representing the ratio of isotopic equilibrium constants were calculated according to the Bigeleisen and Goeppert−Mayer formalism.[51] The usual ideal gas, rigid-rotator, harmonic-oscillator approximation was assumed. The ^{18}O EIE is defined as the product of reduced partition functions corresponding to the isotopic zero point energy (ZPE), vibrational excitation energy (EXC), and the mass and moments of inertia (MMI). Each term was calculated from full sets of vibrational frequencies (ν) of the reactant and product states,[c,52,53] in accord with the Redlich−Teller product rule.[54] Alternatively, the classical contribution designated MMI_{rot} was computed from molecular masses and the principal rotational moments of inertia. Favorable agreement of the MMI and MMI_{rot} calculated using two independent approaches serves as a check on the quality of the DFT-derived structure.[55]

The oxygenated intermediates and products formed by R*α*O contain chemically inequivalent oxygen atoms in positions directly attached to or one atom removed from the *α*-carbon. Thus, a small intramolecular effect exists, which can be computed by considering the relative energies of the two isotopomers. Such effects were neglected in earlier studies[c,52,53,55,65−70] by assuming a 50/50 distribution of ^{18}O in the two positions. This averaging is depicted in the isotope exchange reaction in eq 2, where the asterisk denotes the site of the heavy isotope and the ^{18}O EIE = $^{16,16}K/(^{16,18}K + {}^{18,16}K)/2$. In view of the small isotope effects observed in this study, isotopomeric population differences are explicitly considered for the ^{18}O EIE and ^{18}O KIEs described below.[c]

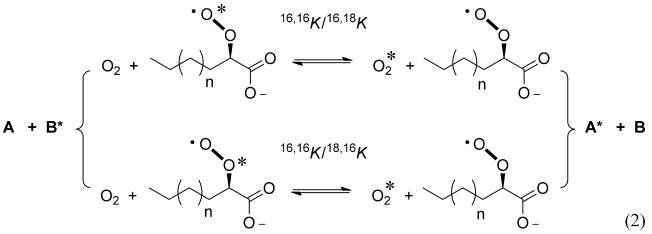

(2)

Wolfsberg and Bigeleisen developed an approach to calculating ^{18}O KIEs based on the tenets of transition state theory (TST) and utilizing the vibrational frequencies of the isotopic reactant and transition states. In eq 3, the ^{18}O KIE is the product of terms corresponding to the isotope effect on the reaction coordinate frequency ($^{18}\nu^{\ddagger}$) and the isotope effect on the pseudoequilibrium constant for attaining the transition state ($^{18}K_{TS}$). The $^{18}\nu^{\ddagger}$ is defined by the ratio of imaginary modes reflecting the decomposition frequency of the TS. The $^{18}K_{TS}$ is calculated in the same manner as the ^{18}O EIE (eq 2);[c] however, the isotope exchange takes place between the reactant O_2 (A) and the transition state (B), which possesses $3N - 7$ vibrational modes. The asterisk designates the site of the heavy isotope in A and B. Other terms in eq 3 include Boltzmann's constant (k), Planck's constant (h), and temperature (T).

$$^{18}\text{O KIE} = \frac{\nu^{\ddagger}_{B}}{\nu^{\ddagger}_{B^*}} \times \frac{\prod_{j}^{3N^{TS}-7} \left(\nu_{j,B}/\nu_{j,B^*}\right) \times \left[\frac{1-e^{-(h\nu_{j,B^*}/kT)}}{1-e^{-(h\nu_{j,B}/kT)}}\right] \times \left[\frac{e^{(h\nu_{j,B^*}/2kT)}}{e^{(h\nu_{j,B}/2kT)}}\right]}{\prod_{i}^{3N-5} \left(\nu_{i,A}/\nu_{i,A^*}\right) \times \left[\frac{1-e^{-(h\nu_{i,A^*}/kT)}}{1-e^{-(h\nu_{i,A}/kT)}}\right] \times \left[\frac{e^{(h\nu_{i,A^*}/2kT)}}{e^{(h\nu_{i,A}/2kT)}}\right]} \quad (3)$$

RESULTS

Previous studies of R*α*O demonstrated that the reversibility of initial hydrogen atom abstraction from the fatty acid is influenced by the concentration of O_2.[18] Reported here are new findings under physiologically relevant conditions, which indicate that O_2-trapping of the *α*-carbon radical is also reversible, and reduction of the 2-(*R*)-peroxyl radical by the catalytic Tyr379 is the turnover limiting step in enzyme catalysis. The results described below reflect upon the mechanism of proton-coupled electron transfer (PCET) as it relates to the turnover-limiting step that generates the 2-(*R*)-hydroperoxide product and regenerates the catalytic Tyr379$^{\bullet}$.

Substrate and Solvent Deuterium Kinetic Isotope Effects. Experiments with three saturated fatty acids were undertaken to probe the microscopic steps contributing to the bimolecular rate constant, $k_{cat}/K_M(O_2)$. Values determined for each of the protiated fatty acids approximate 3×10^5 M^{-1} s^{-1}. In contrast, the $k_{cat}/K_M(FA)$, defined at O_2 saturation, decreases by orders of magnitude upon shortening the fatty acid chain length. Moreover, the corresponding $^{D}k_{cat}/K_M(FA)$ increases from ∼30 to 120, in a manner that is similar to the KIE on the turnover rate constant, $^{D}k_{cat}$. These values, taken to represent intrinsic deuterium kinetic isotope effects, are proposed to be consistent with the increasing C_α−H−O tunneling distances and weakened binding affinities of the fatty acids.[18]

In view of this kinetic mechanism, the deuterium KIEs upon $k_{cat}/K_M(O_2)$ defined at saturating fatty acid concentrations

contain a small contribution from the isotope effect on the pre-equilibrium hydrogen transfer step, $^{D}K_{eq}$ ~1.4.[18] The larger observed $^{D}k_{cat}/K_M(O_2)$ values are most readily explained by reoxidation of Tyr379 by a mechanism of concerted PCET or a sequential variant, where reversible electron transfer precedes rate-limiting proton transfer. As predicted on the basis of slow solvent isotope exchange with Tyr379 under anaerobic conditions, $^{D}k_{cat}/K_M(O_2)$ derives from the hydrogen retained from the fatty acid.

Measurements comparing the oxidation of h_{31}-16:0 to d_{31}-16:0 and α,α-d_2-16:0, shown in Figure 2, indicate

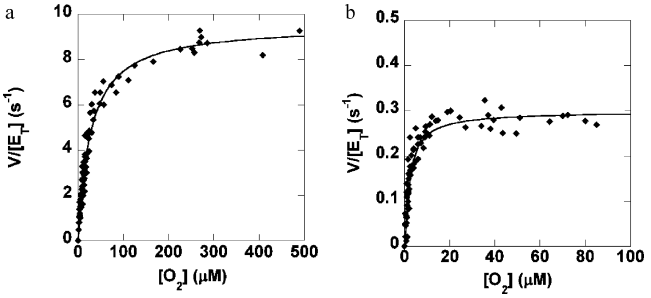

Figure 2. Determination of $^{D}k_{cat}/K_M(O_2)$ for the oxidation of h_{31}-16:0 (a) and d_{31}-16:0 as well as α,α-d_2-16:0 (b) at pH 7.2 and 22 °C.

$^{D}k_{cat}/K_M(O_2)$ = 2.5 ± 0.2 at pH 7.2 and 22 °C. This is the result of the large $^{D}k_{cat}$ ~30 and a diminished $K_M(O_2)$ for the deuterated substrate relative to the protiated substrate. Although the $K_M(O_2)$ is close to the detection limit of the O_2 electrode, the reported results were consistently obtained by multiple researchers using different preparations of RαO as well as fatty acids. In addition, it was verified that preincubation of RαO with H_2O_2 increased the enzyme's dioxygenase activity but did not affect the kinetic constants for 16:0.

For comparison to the ambient temperature results, $^{D}k_{cat}/K_M(O_2)$ was evaluated at a lower temperature, where $K_M(O_2)$ is larger.[17] At pH 7.2 and 6 °C, $^{D}k_{cat}/K_M(O_2)$ = 1.8 ± 0.5 results from $k_{cat}/K_M(O_2)$ values of (6.07 ± 0.86) × 10^4 M^{-1} s^{-1} for h_{31}-16:0 and (3.31 ± 0.86) × 10^4 M^{-1} s^{-1} for d_{31}-16:0. Although the rate constants are smaller than those at 22 °C, the KIE is decreased slightly suggesting the possibility of kinetic complexity.[56,57]

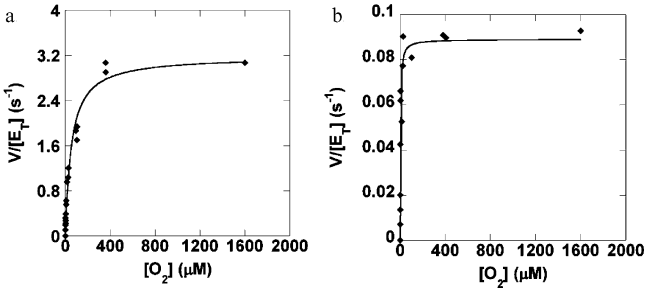

Figure 3. Determination of $^{D}k_{cat}/K_M(O_2)$ for h_{31}-16:0 (a) and d_{31}-16:0 (b) at pH 7.2 and 6 °C.

The solvent kinetic isotope effect, $^{D_2O}k_{cat}/K_M(O_2)$, was initially examined with h_{31}-16:0 at 22 °C to assess the involvement of exchangeable protons bound to Tyr379 in peroxyl radical reduction. The results in Figure 4 reveal

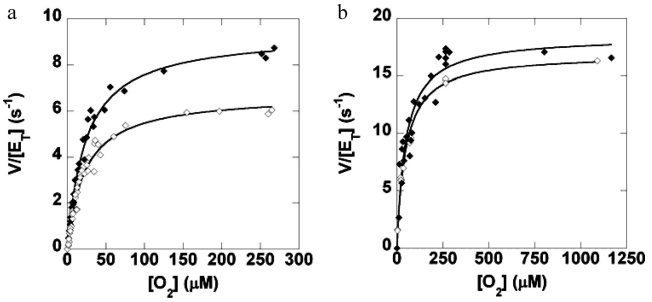

Figure 4. Determination of $^{D_2O}k_{cat}/K_M(O_2)$ at 22 °C with h_{31}-16:0 at pH/pD 7.2 (a) and pH/pD 10.0 (b).

$^{D_2O}k_{cat}/K_M(O_2)$ = 1.3 ± 0.1 at pH 7.2 and 1.1 ± 0.1 at pH 10.0. These values are significantly smaller than the $^{D}k_{cat}/K_M(O_2)$ determined under the analogous conditions. The results are consistent with slow solvent isotope exchange with Tyr379 on the time scale of enzyme turnover.[18] In addition to the somewhat larger solvent isotope effect at pH 7.2, $k_{cat}/K_M(O_2)$ is reduced upon lowering the pH. This behavior suggests the involvement of an active site base; however, conclusive experiments could not be performed due to limited fatty acid solubility. His311 would seem to be a good candidate for the base because of its proximity to Tyr379. This residue could facilitate proton transfer from the reduced tyrosine to the fatty acid-derived 2-(*R*)-peroxide intermediate.

Table 1. RαO-Catalyzed Oxidation of 16:0 (100 μM) at Variable pH and Temperature

temp (°C)	pH	$^{D}k_{cat}/K_M(O_2)^a$	$^{D_2O}k_{cat}/K_M(O_2)^b$
22	10.0	2.1 ± 0.4	1.1 ± 0.1
22	7.2	2.5 ± 0.2	1.3 ± 0.10
6	7.2	1.8 ± 0.3	n.d.[c]

[a]The ratio of $k_{cat}/K_M(O_2)$ determined with h_{31}-16:0 to $k_{cat}/K_M(O_2)$ determined with d_{31}-16:0 or α,α-d_2-16:0. [b]The ratio of $k_{cat}/K_M(O_2)$ for h_{31}-16:0 in H_2O to that in D_2O. [c]Not determined.

Experiments with 12:0 at a concentration of 300 μM, i.e. ~6$K_M(O_2)$, uncover a somewhat larger $^{D}k_{cat}/K_M(O_2)$ than that observed with 16:0 at pH 7.2 and 22 °C. The data depicted in Figure 5 indicate k_{cat} = 13.7 ± 0.8 s^{-1} and

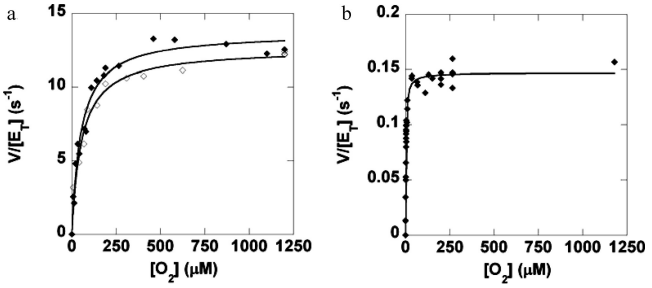

Figure 5. Comparison of $k_{cat}/K_M(O_2)$ for (a) the oxidation of h_{23}-12:0 in H_2O (filled diamonds) and in D_2O (open diamonds) to (b) the oxidation of d_{23}-12:0 in H_2O at pH/pD 7.2 and 22 °C.

$K_M(O_2)$ = 51 ± 12 μM for h_{23}-12:0, whereas k_{cat} = 0.147 ± 0.005 s^{-1} and $K_M(O_2)$ = 2.6 ± 0.4 μM for d_{23}-12:0. The derived $k_{cat}/K_M(O_2)$ = (2.7 ± 0.3) × 10^5 M^{-1} s^{-1} for h_{23}-12:0 and $k_{cat}/K_M(O_2)$ = (5.7 ± 0.3) × 10^4 M^{-1} s^{-1} for d_{23}-12:0 result

dx.doi.org/10.1021/bi201016h | *Biochemistry* 2011, 50, 7375–7389

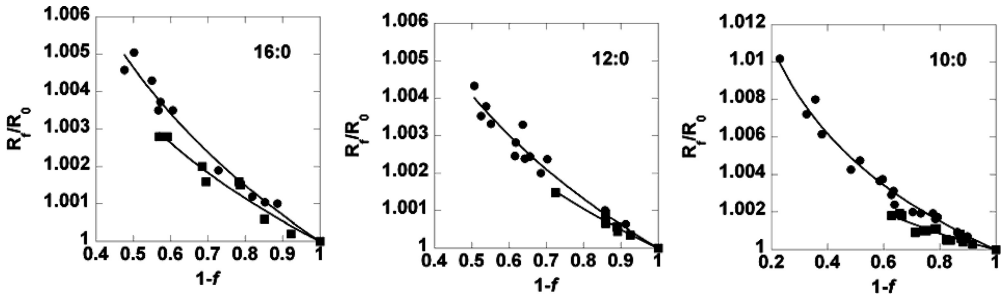

Figure 6. Isotope fractionation plots for protiated (circles) and perdeuterated (squares) fatty acids. The *y*-axis represents ^{18}O enrichment while the *x*-axis represents the O_2 remaining in solution. Curves are fitted to $R_f/R_0 = 1 - f^{(1/\alpha-1)}$ where α is the competitive ^{18}O KIE.

in $^{D}k_{cat}/K_M(O_2)$ = 4.7 ± 0.5. In addition, rate constants determined for h_{23}-12:0 in H_2O and D_2O indicate $^{D_2O}k_{cat}/K_M(O_2)$ = 1.2 ± 0.2 (Figure 5). As with 16:0, the $^{D}k_{cat}/K_M(O_2)$ significantly exceeds the $^{D_2O}k_{cat}/K_M(O_2)$, consistent with isotope effects originating from separate physical processes.

Viscosity Effects as Probes of Diffusion-Controlled Steps. Diffusion-controlled reactions of small molecules such as O_2 can be a challenge to detect because of deviations from the Stokes–Einstein relation.[33,34] Experiments to test the contribution to $k_{cat}/K_M(O_2)$ from an encounter-controlled reaction of O_2 or release of the hydroperoxide product were, therefore, conducted at high relative solution viscosities (η^{rel} = 4.0). These conditions allow for the detection of diffusion-controlled processes in spite of the fractional (~0.5) exponent[33] that has been shown to empirically relate the ratio of rate constants to η^{rel}. These experiments could also expose the contribution to $k_{cat}/K_M(O_2)$ from product release,[58] if all preceding steps were reversible.

Linear regression analysis of the data collected at O_2 concentrations sufficiently below $K_M(O_2)$ indicate $k_{cat}/K_M(O_2) = (3.0 \pm 0.2) \times 10^5$ M^{-1} s^{-1} for a buffer-only solution, in good agreement with the full Michaelis–Menten analysis (cf. Figure 1). This rate constant is indistinguishable from $k_{cat}/K_M(O_2) = (2.9 \pm 0.4) \times 10^5$ M^{-1} s^{-1} determined for solutions containing 7% Ficoll 400 and $k_{cat}/K_M(O_2) = (3.1 \pm 0.3) \times 10^5$ M^{-1} s^{-1} for solutions containing 30% glycerol, for which η^{rel} = 4.[c] That $k_{cat}/K_M(O_2)$ at pH 7.2 and 22 °C is unaffected by increased solution viscosity argues against diffusion-controlled O_2-trapping of the α-carbon radical or release of the hydroperoxide product.

Competitive Oxygen-18 Kinetic Isotope Effects. The competitive ^{18}O KIE probes the same steps which contribute to $k_{cat}/K_M(O_2)$, beginning as O_2 enters the catalytic cycle, leading up to and including the first kinetically irreversible step. The methodology used to prepare samples has been described earlier[36,37] and is discussed briefly in the Experimental Section. Per the standard protocol, the O_2 isolated before and after the enzymatic reaction was quantitatively recovered and then combusted to CO_2. The resulting sample is of identical isotopic content and pressure to the O_2 from which it formed. IRMS analysis of the CO_2 samples provides the isotope ratios, R_0 and R_f, needed for the determination of ^{18}O KIEs at specific fractional conversions, *f*. The isotope fractionation plots in Figure 6 reveal normal ^{18}O KIEs for reactions of the protiated and perdeuterated fatty acids.

The ^{18}O KIEs are summarized along with $k_{cat}/K_M(O_2)$ and $K_M(O_2)$ determined for each of the fatty acids in Table 2. The ^{18}O KIEs vary from 1.0061(7) to 1.0068(8) with the three protiated fatty acids. A slight decrease in the ^{18}O KIEs is indicated by comparison to the perdeuterated fatty acids, which are between 1.0038(9) and 1.0048(10). These results provide evidence that the shortest chain substrate, 10:0, is oxidized by the same mechanism as 12:0 and 16:0, in the absence of measurable $k_{cat}/K_M(O_2)$ and $^{D}k_{cat}/K_M(O_2)$ values.

Table 2. Limiting Kinetic Constants and Competitive ^{18}O KIEs Determined for the RαO-Mediated Oxidation of Fatty Acids at pH 7.2 and 22 °C

substrate	$k_{cat}/K_M(O_2) \times 10^5$ (M^{-1} s^{-1})	$K_M(O_2)$ (μM)	$^{18}k_{cat}/K_M(O_2)$[a]
h_{31}-16:0	3.5 ± 0.2	27 ± 2.6	1.0068 ± 0.0008 (10)
d_{31}-16:0	1.4 ± 0.1	2.1 ± 0.3	1.0048 ± 0.0010 (10)[b]
h_{23}-12:0	2.7 ± 0.3	51 ± 12	1.0061 ± 0.0007 (13)
d_{23}-12:0	0.57 ± 0.03	2.6 ± 0.4	1.0047 ± 0.0007 (7)
h_{19}-10:0	>1.8[c]	31 ± 5.0	1.0066 ± 0.0007 (18)
d_{19}-10:0	>0.64[d]	n.d.[e]	1.0038 ± 0.0009 (15)[b]

[a]The number of independent measurements used to determine the ^{18}O KIE is given in parentheses. [b]Includes data measured by preincubating RαO with H_2O_2. [c]The $^{ap}k_{cat}/K_M(O_2)$ at 750 μM h_{19}-10:0 is taken as a lower limit. [d]Data collected at 200 μM d_{19}-10:0. [e]Not determined.

Computational Analysis. DFT calculations using the modified Perdew–Wang functional (*m*PW91) and the 6-311+G-(2df,p) basis set were undertaken to locate various intermediate and transition state structures. This functional/basis set choice was motivated by its ability to quantitatively reproduce the experimental O–O stretching frequency, and the associated ^{18}O isotope shift, of molecular O_2. In addition, the DFT method has been calibrated and shown to reproduce ^{18}O EIEs on reactions of O_2 that reversibly produce transition metal superoxo, peroxo, and hydroperoxo structures.[c,52,53]

The ^{18}O EIEs were computed for the 2-peroxyl, 2-peroxide, and 2-hydroperoxide derivatives of the methylbutanoate ester, which serve as models of potential intermediates during RαO catalysis (Table 3). Separate calculations were performed for the reactions in the gas and condensed phases at 22 °C to assess the influence of a dielectric environment (ε_s = 78.3 for H_2O). The unlabeled esters were selected to avoid intramolecular hydrogen bonding of the 2-hydroperoxide moiety to the carboxylate group noticed for the parent fatty acid. The resulting ^{18}O EIEs are characteristic of the ground state structures and in the above-mentioned cases differ significantly from the measured ^{18}O KIEs; normal ^{18}O EIEs characterize the formation of 2-peroxide compounds, whereas inverse effects characterize the formation of 2-peroxyl and 2-hydroperoxide compounds. Increasing the dielectric of the environment had a negligible effect on the computed ^{18}O EIEs in contrast to the computed ^{18}O KIEs (described below).

dx.doi.org/10.1021/bi201016h | *Biochemistry* 2011, 50, 7375–7389

Table 3. ^{18}O EIEs upon Formation of Peroxyl, Peroxide, and Hydroperoxide Structures from O_2 and R$^\bullet$ (R = Methyl Butanoate), Computed at the *m*PW/6-311+G(2df,p) Level of Theory

product	phase[a]	ZPE[b]	EXC[b]	MMI[b]	MMI$_{rot}$[c]	EIE[d]
ROO$^\bullet$	gas	0.9498	0.9489	1.1078	1.1074	0.9978
	H_2O[e]	0.9484	0.9479	1.1106	1.1075	0.9979
d_6-ROO$^\bullet$	gas	0.9486	0.9481	1.1099	1.1095	0.9975
	H_2O[e]	0.9473	0.9475	1.1120	1.1096	0.9976
ROO$^-$	gas	0.9471	0.9535	1.1132	1.1128	1.0051
	H_2O[e]	0.9551	0.9505	1.1098	1.1069	1.0065
d_6-ROO$^-$	gas	0.9458	0.9527	1.1153	1.1150	1.0048
	H_2O[e]	0.9538	0.9498	1.1118	1.1090	1.0061
ROOH	gas	0.9350	0.9555	1.1088	1.1085	0.9901
	H_2O[e]	0.9379	0.9404	1.1260	1.1083	0.9926
d_6-ROOD	gas	0.9274	0.9559	1.1117	1.1114	0.9852
	H_2O[e]	0.9303	0.9415	1.1281	1.1113	0.9876

[a]The gaseous and aqueous phases represent two extreme limits. [b]Reduced isotopic partition functions defined in the Supporting Information. [c]Newtonian expression for MMI$_{rot}$ is provided in the Supporting Information. [d]Product of columns 3, 4, and 5. [e]Aqueous solvation within the SMD model.

To test the effect of external hydrogen-bonding, the 2-peroxyl and 2-hydroperoxide bound to h_6- and d_6-butanoate fragments were considered to interact with isotopically labeled 4-methylphenol.[c] The interaction was found to confer stabilization and increase the ^{18}O EIEs in both cases. Only in the case of the 2-peroxyl radical did hydrogen bonding increase the ^{18}O EIE from inverse to slightly above unity; the ^{18}O EIEs for the 2-hydroperoxide compounds remain inverse.

^{18}O KIEs were computed at the same level of theory as the ^{18}O EIEs.[b] In each case, the TS was defined by a single isotopic imaginary mode. It has been widely assumed that ^{18}O EIEs represent upper limits to ^{18}O KIEs on reactions where the O−O bond is not made or broken.[c,52,53,59−62] This assumption can be traced back to the statistical mechanical formulation of KIEs according to transition state theory as well as the analogies often drawn between heavy atom isotope effects and secondary isotope effects.[59−64] While such approximations appear to hold for certain types of reactions, such as the coordination of O_2 to a redox metal,[c,52,53,65,66] failures are expected when O−O vibrations contribute to the reaction coordinate.[67] In the present studies, small normal ^{18}O KIEs are observed for concerted PCET reactions characterized by inverse ^{18}O EIEs. It remains to be seen how the theoretically predicted relationships between ^{18}O KIEs and ^{18}O EIEs apply to other types of PCET reactions, such as those involving transition metal−O_2 adducts.[68,69]

The goal of this study, in part, was to determine how perturbations in the distance between reacting components and the environmental polarity influence ^{18}O KIEs on concerted PCET reactions from Tyr379 to an O_2-derived 2-(*R*)-peroxyl radical, forming the Tyr379$^\bullet$ and the 2-(*R*)-hydroperoxide product. The computed ^{18}O KIEs summarized in Table 4 are associated with concerted mechanisms, with both proton and electron transfer occurring in a single step, as opposed to sequential mechanisms which proceed via high-energy intermediates.

One example of sequential PCET involves reversible endoergic electron transfer from Tyr379 to the 2-(*R*)-peroxyl radical, followed by rate-limiting proton transfer to form the Tyr379$^\bullet$ and 2-(*R*)-hydroperoxide product. Because of the inverse contribution from the KIE on proton transfer, such reactions are expected to exhibit normal ^{18}O KIEs that are somewhat smaller than the ^{18}O EIEs on the pre-equilibrium step. Another example involving reversible endoergic proton transfer from Tyr379 to the 2-(*R*)-peroxyl radical, followed by rate-limiting electron transfer, should be characterized by an ^{18}O KIE that is larger than the ^{18}O EIE of ∼0.985 estimated from values in Table 3. This hypothetical reaction is inconsistent with both the significant deuterium KIEs and normal ^{18}O KIEs observed. Other alternatives, occurring by initial irreversible electron or proton transfer, are also inconsistent with the observed deuterium and ^{18}O KIEs.

Arguably, none of the sequential mechanisms is consistent with the lack of variation in $k_{cat}/K_M(O_2)$ when the pH is raised from 7.2 to 10.0. The kinetics of concerted PCET is unlikely to be influenced by changing solution pH as long as no residues are protonated or deprotonated. Such mechanisms are much more favorable than the sequential alternatives, regardless of whether the electron localizes on the transferring proton, as in "hydrogen atom transfer", or whether the proton and electron exhibit separate trajectories but transfer in the same kinetic step, as depicted in Figure 1.

To simulate the influence of a polarized active site environment upon the kinetic ^{18}O KIEs, the dielectric constant was changed from gaseous to aqueous phase. This variation is not meant to imply that the enzyme active site is characterized by such a small or large dielectric constant, but merely to assess the effects at the nonpolar and polar extremes. Geometric constraints were also imposed on the donor−acceptor distance. ^{18}O KIEs were calculated in the gas phase for separations of oxygen atoms (R_{O-O}) from 2.7 to 3.3 Å,[c] which are significantly greater than the optimized distance in the unconstrained gas and aqueous transition state (TS) structures, where the separations between the distal peroxyl and the tyrosyl oxygen atoms are 2.409 and 2.425 Å, respectively.

Calculations designed to explore the influence of reactant separation reveal that when R_{O-O} is lengthened from 2.7 to 3.3 Å, the ^{18}O KIE increases from ∼0.998 to ∼1.004, in a manner that depends weakly upon the transferring hydrogen isotope.[c]

Table 4. ^{18}O KIEs Derived from Transition States for Net Hydrogen Atom Transfer from 4-Methylphenol (ArOH or ArOD) to 2-Peroxyl Methylbutanoate (h_6- or d_6-ROO$^\bullet$)[a]

TS structure[b]	ZPE	EXC	MMI	MMI$_{rot}$	$^{18}K_{TS}$	$^{18}\nu^{\ddagger}$ (cm^{-1})	^{18}O KIE
ROO$^\bullet$--**H**OAr	0.9295	0.9358	1.1411	1.1431	0.9923	1.0018	0.9941
d_6-ROO$^\bullet$--**D**OAr	0.9285	0.9363	1.1418	1.1439	0.9924	1.0019	0.9942
ROO$^\bullet$--**H**OAr (H_2O)	0.9393	0.9372	1.1354	1.1434	0.9991	1.0058	1.0049
d_6-ROO$^\bullet$--**D**OAr (H_2O)	0.9393	0.9371	1.1367	1.1442	1.0002	1.0058	1.0060

[a]Optimized structures were calculated at the *m*PW/6-311+G(2df,p) level of theory in the gas phase or an aqueous continuum model (SMD). The ^{18}O KIEs are the products of $^{18}\nu_{RC}$ and $^{18}K_{TS}$ (eq 3). [b]Comparisons to constrained structures are provided in the Supporting Information.

dx.doi.org/10.1021/bi201016h | *Biochemistry* 2011, 50, 7375−7389

The computational results demonstrate that both the high dielectric environment and increased distance between the peroxyl radical and the reduced tyrosine, beyond the ~2.4 Å associated with the optimized TS structure, lead to increasingly normal KIEs. Thus, if interactions within the enzyme were to hold the reacting species at a larger separation distance than computed for an isolated system (i.e., 2.7−3.3 Å), this would counter any tendency toward decreasing the ^{18}O KIE in association with decreasing the active site dielectric.

In addition, the calculated ^{18}O KIEs on concerted PCET consistently follow the trend $d_1 > d_7 > h_7$ as a result of competing influences due to the R_{O-O} distance and deuterium substitution of the carbon backbone. The trend is maintained over all distances investigated in the gas phase where 0.9984 (d_1) > 0.9980 (d_7) > 0.9978 (h_7) at 2.7 Å, 1.0019 (d_1) >1.0016 (d_7) > 1.0014 (h_7) at 3.0 Å, and 1.0044 (d_1) > 1.0040 (d_7) > 1.0038 (h_7) at 3.3 Å.[c] The same trends are observed for the unconstrained structures in the gaseous and aqueous phases, even when corrections for intramolecular isotope effects are applied.[c]

Calculations of ^{18}O isotope effects have typically neglected intramolecular isotope effects, which derive from the population differences due to the preferred coordination mode of $^{16,18}O_2$.[c,52,53,55,59−62,67−69] Given the small differences in ^{18}O KIEs observed experimentally and computationally, an analysis was undertaken to correct for the relative isotopomeric energies of intermediates and transition states. As expected, the intramolecular isotope effects are found to be minor compared to the intermolecular isotope effects when appropriately weighted by the isotopomeric energy differences.[c] Localization of ^{18}O at C_α, the position associated with the greatest force constant, is consistently observed for all oxygenated species with the exception of the hydroperoxide products in which the ^{18}O bonded to the H dominates. The other ^{18}O EIEs and KIEs are uniformly decreased relative to the values computed assuming a 50/50 distribution of the isotopomers (cf. Tables 3 and 4). Interestingly, the correction is largest for the anionic peroxide intermediate, with the magnitude depending on whether its structure was optimized in the gas phase or in a dielectric continuum.[c]

Summary of Computational Results. The computational results are described in more detail below, but it suffices to note here a few of the trends. (i) The ^{18}O EIEs for species in Table 3 all increase slightly with increasing polarity. This effect derives from the O−O bonds all being shorter (and stronger) for the structures optimized in the aqueous medium, presumably owing to better stabilization of the partial negative charge that concentrates on and otherwise decreases the bonding interaction between the electronegative oxygen atoms. (ii) The ^{18}O EIEs on formation of deuterated peroxyl radicals or peroxides are slightly smaller than the ^{18}O EIEs on reactions of the protiated derivatives. The opposite is predicted for the ^{18}O KIEs, where the deuterated transition states exhibit isotope effects larger than the protiated transition states. The slight trends between h_7, d_7, and d_1 isotopologues characterize all of the ^{18}O KIEs calculated in this study. (iii) Compared to the gas phase, the fully optimized transition state structure in condensed phase (H_2O) reveals that electron transfer is more advanced than proton transfer. In the condensed phase, the breaking O−H bond is 1.130 Å and the forming O−H bond is 1.303 Å. By contrast, in the gas phase, the breaking O−H bond is 1.205 Å (0.075 Å longer) and the forming O−H bond is 1.210 Å (0.093 Å shorter), leading to a more symmetric structure than those in aqueous medium. This difference results in the prediction that ^{18}O KIEs are inverse in the gas phase and normal in solution. The ratio of ^{18}O KIEs for solution phase reactions versus gas phase reactions, which is ~1.01, can be almost entirely attributed to a less inverse ZPE contribution in the condensed phase. Thus, the ^{18}O KIE is predominantly associated with bound normal modes and, to a lesser extent, the imaginary mode defining the reaction coordinate. (iv) Effects similar to those noted above lead to increasingly normal KIEs as the O−O separation in the precursor complex increases. This variable is considered only for the gas phase structures but should result in the same trend in solution, increasing the KIE by ca. 0.01 over the range of almost 0.9 Å considered. (v) Finally, the calculations reveal a slight trend where ^{18}O KIEs on concerted PCET decrease in the order $d_1 > d_7 > h_7$. This behavior, seen in both gas and condensed phases, arises from competing effects where the size of the ^{18}O KIE due to increased O--(H/D)--O separation is attenuated by deuterium substitution of the carbon backbone. It is important to note, however, that the computed trends are at least an order of magnitude smaller than the experimental variations compiled in Table 2.

DISCUSSION

RαO is an ideal model system for examining the PCET mechanisms by which fatty acids are regio- and stereospecifically oxidized using a tyrosyl radical. These reactions produce oxylipins which control numerous physiological processes, from cell signaling, wound healing and pathogen resistance in plants to inflammation and immunity in mammals. The reactivity of other fatty acid dioxygenases, such as the cyclooxygenases[70,71] and lipoxygenases,[72,73] is more complicated due to allosterism, multiple reactive configurations of substrates, and deactivation events that result from accumulation of the hydroperoxide products required to initiate catalysis. By comparison, RαO exhibits simple kinetic behavior partly because of the spontaneous (nonenzymatic) decarboxylation of the 2-hydroperoxide product upon its release from the active site.

Previous studies of RαO illuminated the kinetic mechanism and the quantum mechanical features of the Tyr379$^\bullet$-mediated C_α−H homolysis step at saturating O_2 concentrations.[17,18] The large intrinsic substrate deuterium KIEs due to nuclear tunneling undergo a hyperbolic decrease, from limiting values of 30 (16:0) to 120 (10:0), upon decreasing the concentration of O_2 in the physiological range (<30 μM). This behavior indicates that initial hydrogen atom abstraction from the fatty acid is reversible and a downstream step limits enzyme turnover.

The $k_{cat}/K_M(O_2)$ exhibited by RαO of ~3×10^5 M^{-1} s^{-1} is comparable to those reported for the fatty acid dioxygenases mentioned above.[70−77] On the basis of DFT calculations, small inverse ^{18}O EIEs are expected for O_2-trapping steps leading to peroxyl radicals. Subsequent reduction to an anionic peroxide is characterized by a moderately sized normal ^{18}O KIE closer to the values of 1.0110(16) and 1.0133(20) reported for the oxidation of linoleic acid by soybean lipoxygenase[75,76] and cyclooxygenase-1.[77] These ^{18}O KIEs are within error of one another but significantly larger than those observed in RαO, suggesting a fundamental difference in the PCET mechanism.

Proton-Coupled Electron Transfer in RαO. Scheme 2 depicts two possible reaction sequences that account for the

Scheme 2. Mechanisms of Concerted and Sequential Proton-Coupled Electron Transfer[a]

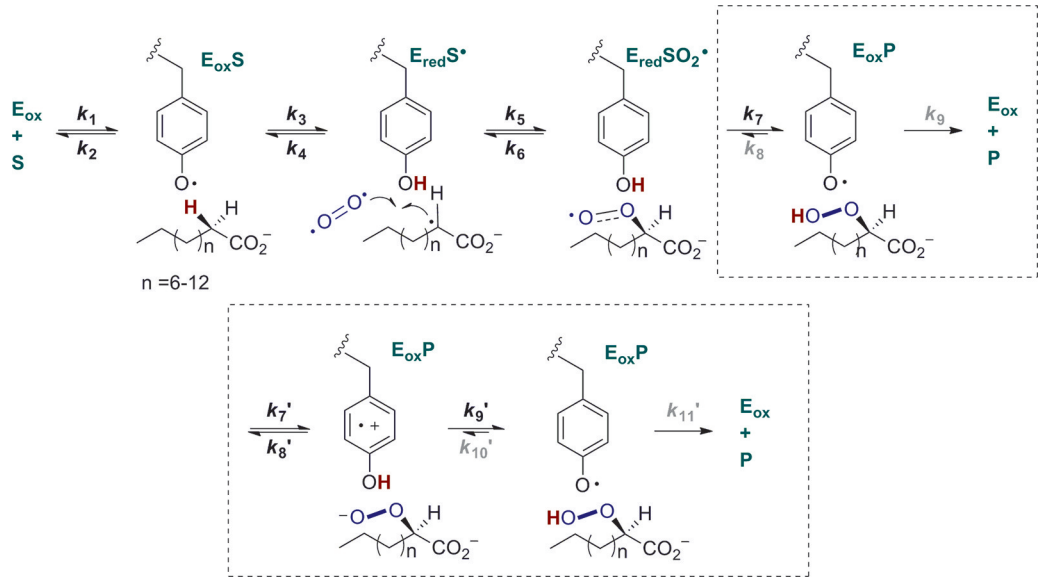

[a]Note that steps leading up to formation of the 2-(*R*)-peroxyl radical are the same in both pathways.

observed $^{D}k_{cat}/K_M(O_2)$ and ^{18}O KIEs observed in RαO. In the upper pathway, concerted PCET occurs in the first kinetically reversible step (k_7), followed by more rapid release of the 2-(*R*)-hydroperoxide product (k_9) than the rate constant for reverse PCET (k_8). In the lower pathway, a sequential mechanism is considered involving reversible electron transfer (k_7'/k_8') prior to proton transfer (k_9') in the first irreversible and rate-limiting step. Although there are other types of sequential PCET mechanisms, the sequence shown above uniquely accounts for the observations of normal ^{18}O KIEs and deuterium KIEs on $k_{cat}/K_M(O_2)$ in RαO.

Interpretation of Deuterium Kinetic Isotope Effects.

Two types of deuterium KIEs, $^{D}k_{cat}/K_M(O_2)$ and $^{D_2O}k_{cat}/K_M(O_2)$, defined at saturating fatty acid concentrations have been determined in this study. The $^{D}k_{cat}/K_M(O_2)$ observed upon comparing rate constants for protiated substrates to perdeuterated or α,α-dideuterated substrates provides the main evidence that reversible O_2-trapping of a fatty acid-derived α-carbon radical precedes peroxyl radical reduction by Tyr379 in the first irreversible step.

Several trials with the native substrate (16:0) at pH 7.2 consistently demonstrated a small but significant $^{D}k_{cat}/K_M(O_2)$ = 2.5 ± 0.2 at 22 °C. Upon lowering the temperature to 6 °C, $^{D}k_{cat}/K_M(O_2)$ = 1.8 ± 0.3 is marginally reduced. This result is more likely to signal kinetic complexity than an inverse temperature dependence of the primary deuterium KIE.[56,57] Under the same conditions, a small solvent deuterium KIE of $^{D_2O}k_{cat}/K_M(O_2)$ = 1.3 ± 0.1 is observed on the oxidation of h_{31}-16:0. The effect becomes negligible as the pH/pD is raised to 10.0, i.e., $^{D_2O}k_{cat}/K_M(O_2)$ = 1.1 ± 0.1, whereas the $^{D}k_{cat}/K_M(O_2)$ = 2.1 ± 0.4 remains significantly larger than the equilibrium isotope effect upon the initial hydrogen abstraction step, for which $^{D}K_{eq} \sim 1.4$ has been calculated.[18]

The disparate substrate and solvent KIEs are consistent with results of earlier studies, which suggested slow solvent exchange with the active site Tyr379, resulting in the retention of the hydrogen atom abstracted from the α-position of the fatty acid. This hydrogen is rapidly transferred to the 2-(*R*)-peroxyl radical intermediate accounting for the apparent inhibition of isotope scrambling between the fatty acid and solvent in the presence of O_2.[18]

Experiments with the intermediate chain-length fatty acid (12:0) indicate $^{D}k_{cat}/K_M(O_2)$ = 4.7 ± 0.5 at pH 7.2. Again, the $^{D}k_{cat}/K_M(O_2)$ is substantially larger than $^{D_2O}k_{cat}/K_M(O_2)$ = 1.2 ± 0.1, confirming that the substrate and solvent deuterium KIEs have different origins. While $^{D}k_{cat}/K_M(O_2)$ reflects reduction of the 2-(*R*)-peroxyl radical by Tyr379(O−H/D), the $^{D_2O}k_{cat}/K_M(O_2)$ suggests a contribution from an as yet unidentified solvent exchangeable site.

The determination of $^{D}k_{cat}/K_M(O_2)$ with 10:0 has not been possible because $K_M(h_{19}$-10:0) is inflated above the limit of fatty acid solubility and $K_M(O_2)$ with d_{19}-10:0 is diminished to the point of immeasurability. Though earlier studies have indicated that $^{D}k_{cat}/K_M$(10:0) = 120 arises from an increased C−H/D--$^{\bullet}$OTyr transfer distance relative to 12:0 and 16:0, each of these reactions becomes reversible at subsaturating O_2 concentrations, resulting in $k_{cat}/K_M(O_2)$ values that are indistinguishable for the protiated substrates. The presence of similar mechanisms is further corroborated by the ^{18}O KIEs, where $^{18}k_{cat}/K_M(O_2)_H$ and $^{18}k_{cat}/K_M(O_2)_D$ show similar values for 10:0, 12:0, and 16:0 (Table 2).

The $^{D}k_{cat}/K_M(O_2)$ expressed according to eq 4 is interpreted for the pathways presented in Scheme 2. In the (upper) concerted PCET pathway, the intrinsic $^{D}k_{PCET} = {}^{D}k_7$ and the forward commitment to catalysis $C_f = (k_7/k_6)(1 + k_5/k_4)$. For the (lower) sequential PCET pathway, $^{D}k_{PCET} = {}^{D}k_9'$ and $C_f = (k_9'/k_8')(1 + k_7'/k_6 + k_5/k_4)$. The reverse commitment to catalysis (C_r) that modifies the equilibrium constant associated with the first irreversible step (K_{PCET}) is negligible under the reaction conditions. This assumption is validated by the observed deuterium KIEs and ^{18}O KIEs upon $k_{cat}/K_M(O_2)$, together with the absence of viscosity effects on this parameter.

dx.doi.org/10.1021/bi201016h | *Biochemistry* 2011, 50, 7375–7389

It follows that eq 4 can be simplified as shown below:

$$ {}^{D}\frac{k_{cat}}{K_M}(O_2) = \frac{{}^{D}k_{PCET}\left({}^{D}\left(\frac{k_3}{k_4}\right)\right) + C_f + {}^{D}(K_{PCET})C_r}{1 + C_f + C_r} \cong \frac{{}^{D}k_{PCET}\left({}^{D}\left(\frac{k_3}{k_4}\right)\right) + C_f}{1 + C_f} \quad (4) $$

According to Scheme 2, the observed ${}^{D}k_{cat}/K_M(O_2)$ from 2.5 to 4.7 may be attributed to intrinsic differences in the hydrogen/hydronium ion transfer probability or kinetic complexity in either the concerted or sequential PCET pathways. Although the $k_{cat}/K_M(O_2)$ values are indistinguishable for the protiated fatty acids (Table 2), the C_f in eq 4 could result in significant changes in ${}^{D}k_{cat}/K_M(O_2)$. Such kinetically complex behavior may explain why ${}^{18}k_{cat}/K_M(O_2)_H$ exceeds ${}^{18}k_{cat}/K_M(O_2)_D$; however, the variation is small in comparison to those predicted for the rate-limiting formation of peroxyl and peroxide intermediates. Furthermore, the minor differences in ^{18}O KIEs can be reproduced computationally by varying the active site dielectric constant as well as the R_{O-O}.

Analysis of Oxygen-18 Kinetic Isotope Effects. Competitive ^{18}O KIEs are predicted here for the first time using transition state structures from high-level DFT calculations. Three different fatty acids have been examined experimentally and average values of ${}^{18}k_{cat}/K_M(O_2)_H \sim 1.0065$ and ${}^{18}k_{cat}/K_M(O_2)_D \sim 1.0044$ determined for three fatty acid substrates. Although the isotopic differences barely exceed the limits of error, they are observed consistently, as expected for rate-limiting hydrogen atom or hydronium ion transfer. The ^{18}O KIEs, which lie outside the range of calculated ^{18}O EIEs on formation of peroxyl and peroxide intermediates by sequential PCET, are reproduced using a DFT-derived transition state for concerted PCET in a polarized (high dielectric) medium. The differences are, however, anticipated to be irresolvable for protium versus deuterium transfer.

Because this is a first-of-a-kind analysis of O_2 reactivity, the "multiple isotope method" outlined by Cleland, O'Leary, and co-workers[78] is applied to estimate potential contributions from kinetic complexity. Solving simultaneous equations, using the heavy atom KIEs for the protiated and deuterated substrates, intrinsic values are approximated assuming the rule of the geometric mean.[64] This rule states there are no isotope effects upon isotope effects because of their independent and cumulative nature.

The relationship between ^{18}O KIEs for protiated and deuterated substrates reacting with RαO depends on whether the isotope effects arise from a single step or from multiple steps related by sequential equilibria.[79] Considering the first situation, deuteration of the substrate should make the isotope-sensitive step more rate-limiting, causing the ^{18}O KIE to be more fully expressed. Alternatively, if the hydrogen-isotope sensitive step were to occur before the oxygen-isotope sensitive step, substrate deuteration is expected to decrease the expression of the ^{18}O KIE.

The analysis below considers whether isotope effects resulting from kinetic complexity are reconcilable with the differences in ^{18}O KIEs observed for the protiated and deuterated substrates, together with the primary deuterium KIEs of 2.5 (16:0) and 4.7 (12:0). Equation 5 was previously derived for a linear multistep mechanism where more than one reaction step gives rise to $^{18}O/^{16}O$ discrimination.[80,81] The result is a product of intrinsic pre-equilibrium and kinetic isotope effects ($^{18}K^{18}k$).[83] With regard to Scheme 2, $^{18}K^{18}k$ reflects the pre-equilibrium isotope effect on O_2 trapping the α-carbon radical followed by reduction of the putative peroxyl radical by PCET. The corresponding isotope effects are ${}^{18}(k_5/k_6)({}^{18}k_7)$ and ${}^{18}(k_5'/k_6'){}^{18}(k_7'/k_8')({}^{18}k_9')$ for concerted and sequential mechanisms, respectively.

$$ {}^{18}K^{18}k \cong \frac{{}^{D}\frac{k_{cat}}{K_M}(O_2)\left({}^{18}\frac{k_{cat}}{K_M}(O_2)_D\right) - {}^{18}\frac{k_{cat}}{K_M}(O_2)_H}{{}^{D}\frac{k_{cat}}{K_M}(O_2) - 1} \quad (5) $$

Application of the multiple isotope effect approximation is most accurate when the variation in ${}^{D}k_{cat}/K_M(O_2)$ is large and the error in this parameter is relatively small.[81] Solving eq 5 using ${}^{D}k_{cat}/K_M(O_2) = 2.5 \pm 0.2$, ${}^{18}k_{cat}/K_M(O_2)_H = 1.0068 \pm 0.0008$, and ${}^{18}k_{cat}/K_M(O_2)_D = 1.0048 \pm 0.0010$ obtained for 16:0 oxidation indicates ${}^{18}K^{18}k = 1.0035 \pm 0.0014$. Extending the analysis to 12:0 using ${}^{D}k_{cat}/K_M(O_2) = 4.7 \pm 0.5$, ${}^{18}k_{cat}/K_M(O_2)_H = 1.0061 \pm 0.0007$, and ${}^{18}k_{cat}/K_M(O_2)_D = 1.0047 \pm 0.0007$ results in ${}^{18}K^{18}k = 1.0043 \pm 0.0008$. These values are slightly smaller than the ^{18}O $KIE_{calc} \approx 1.0055$ for reversible O_2-trapping of the α-carbon radical followed by concerted PCET. Considering the intramolecular isotope effect reduces the ^{18}O KIE_{calc} from 1.0049 (H) and 1.0060 (D) to 1.0047 (H) and 1.0058 (D), consistent with the experimental results.

In contrast to concerted PCET, the boundary limits of ^{18}O KIEs on O_2 coordination and sequential PCET are estimated based on ^{18}O EIEs for the pre-equilibrium formation of intermediates from O_2. The ^{18}O EIE_{calc}, reflecting reversible 2-peroxyl radical formation, is isotopically insensitive, with values of 0.9979 (H) and 0.9976 (D). The isotope effect on subsequent proton transfer to form the peroxyl radical cation is expected to be even more inverse.[78] On the basis of the ${}^{D}k_{cat}/K_M(O_2)$, peroxyl radical formation preceding reversible proton transfer and rate-limiting electron transfer can be excluded in RαO. Although this is not rigorously true for peroxyl radical formation preceding reversible electron transfer and rate-determining proton transfer, the upper limit to the ^{18}O KIE is expected to be the ^{18}O EIE_{calc} on forming the 2-peroxide intermediate. The ^{18}O EIE_{calc}, corrected for intramolecular isotope effects, range from 1.0055(H) and 1.0051(D) in aqueous phase to 1.0048(H) and 1.0045(D) in the gas phase.

It may be surprising that the ^{18}O KIEs calculated for concerted PCET transition from normal to inverse upon decreasing the medium dielectric. This behavior derives from charge redistribution in the transition state, as described below. A similar transition state might be expected for proton transfer subsequent to reversible electron transfer; however, this could not be addressed by the DFT calculations. Such a charge-separated species corresponds to an electronically excited adiabatic state derived from the peroxyl radical and tyrosine (i.e., $ROO^{\bullet}/HOAr \rightarrow ROO^{-}/HOAr^{\bullet+}$). It follows that the ^{18}O KIE should contain a pre-equilibrium contribution estimated for electron transfer, as above, along with a contribution from proton transfer that is inverse and quite small, given its early nature resulting from highly favorable thermodynamics. Although sequential PCET cannot be distinguished from concerted PCET on

the basis of the ^{18}O KIE, this mechanism is unlikely because it requires extensive stabilization of a high-energy intermediate.

Thermodynamic Considerations. The predominance of concerted over sequential PCET mechanisms has been rationalized on thermodynamic grounds.[83,84] Calculating the free energy for reversible electron transfer between Tyr379 and an α-peroxyl radical in RαO gives a pH-independent redox potential of $E^{\circ\prime} \cong 0.77$ V vs NHE for production of the peroxide intermediate.[85] This potential is much less positive than the $E^{\circ\prime} \cong 1.5$ V needed to oxidize Tyr to a $Tyr^{\bullet+}$.[86] Initial electron transfer is, therefore, disfavored by $\Delta E^{\circ\prime} = -0.73$ V, which amounts to $\Delta G^{\circ} = 16.8$ kcal mol^{-1}. Although thermodynamically prohibitive, hydrogen bonding of tyrosine to a nearby base may attenuate the barrier to O−H homolysis.[87]

In RαO, the $k_{cat}/K_M(O_2)$ is associated with a $\Delta G^{\ddagger} = 7.5$ kcal mol^{-1}.[d] This value is comparable to the activation free energy of ~8.4 kcal mol^{-1} computed for concerted PCET over a 2.7 Å O−O separation distance in the gas phase. Further lowering of the $\Delta G^{\ddagger}$ for outer-sphere oxidation of Tyr379 may derive from hydrogen bonding[87] or from electrostatic stabilization by a negatively charged residue. While such effects are difficult to quantify, electrostatic "work" terms for the reactant and product complexes (w_r or w_p) are typically used to estimate the effective free energy for electron transfer according to $\Delta G^{\circ\prime} = \Delta G^{\circ} + w_p - w_r$. Because the peroxyl radical and tyrosine are neutral, $w_r = 0$ kcal mol^{-1} and the stabilizing effect must derive from w_p.

A simple electrostatic model frequently used in electron transfer theory[88] predicts that $w_p = (e^2 z_1 z_2 f_{12})/(\varepsilon_s r_{12})$. In this treatment, the terms include the electron permittivity in vacuum ($e^2 = 332.1$ kcal mol^{-1}), the point charges of the products (z_1 and z_2), the screening factor for these charges ($f_{1,2}$), the static dielectric constant of the surroundings (ε_s) and the inter-reactant distance ($r_{1,2}$). The w_p is smaller in a medium of higher dielectric. Therefore, a low ε_s is required to make the electrostatic correction large enough so that initial electron transfer is not thermodynamically prohibited. Reducing ε_s to a reasonable value of 10, while assuming $f_{1,2} = 1$ and $r_{1,2} = 3.3$ Å, results in a −10 kcal mol^{-1} correction, making $\Delta G^{\circ\prime}$ almost equal to $\Delta G^{\ddagger}$.

Despite the possibility that electrostatics stabilize an initial intermediate formed by reversible electron transfer, neither the magnitude of $k_{cat}/K_M(O_2)$ nor $^{D}k_{cat}/K_M(O_2)$ changes substantially upon raising the solution pH from 7.2 to 10.0. These conditions would be expected to facilitate some degree of Tyr379 deprotonation, thus making electron transfer to the 2-(*R*)-peroxyl radical from the tyrosinate significantly more favorable. The insensitivity of the kinetics argues that the pK_a of Tyr379 is inaccessible at pH 10.0. While this is somewhat unexpected, it may be the result of a hydrophobic active site, which is sequestered from the aqueous solvent. The possibility that another residue provides electrostatic stabilization of a high-energy intermediate is also unlikely because of the pH/pD independent kinetics in the neutral to basic regime.

Overall, the experimental observations are more readily explained by a concerted PCET mechanism. In this case, comparable bond dissociation free energies of the catalytic tyrosine, D(TyrO−H) = 85−90 kcal mol^{-1} and of the 2-(*R*)-hydroperoxide product, D(ROO−H) = 87−92 kcal mol^{-1}, make ΔG° for hydrogen atom transfer close to thermoneutral.[89] The resulting $\Delta G^{\circ} \cong 0$ kcal mol^{-1} is fully consistent with the observed $\Delta G^{\ddagger}$.

Additional Characterization of the Transition State. It is instructive to examine how the proton and electron are coupled in the optimized transition state (TS) for concerted PCET and to characterize how a high dielectric medium affects the TS geometry and its electronic structure. Figure 7 depicts

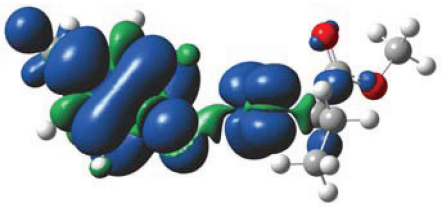

Figure 7. Computed spin density (0.004 au) for the *m*PW91 gas-phase TS structure for concerted PCET; the tyrosyl fragment is shown to the left of 2-peroxymethyl butanoate. The blue and green contours denote regions of positive and negative spin density, respectively.

the spin density in the gas-phase TS structure. It is apparent that electron transfer decreases the unpaired spin density on the peroxyl fragment with concomitant buildup of such density in the π system of the incipient tyrosyl radical. Moreover, negligible spin density is associated with the transferring proton.

The net spin populations on the tyrosyl and peroxyl radical structures from Mulliken analysis in the gas phase (which should be robust here as the overlap between the two structures is essentially zero) are 0.56 and 0.44, respectively. Thus, in light of the optimized gas phase TS structure, it is appropriate to describe this reaction as a proton-coupled electron transfer, where the H^+ and e^- are transferred to or from different sites, rather than as a hydrogen atom ($H^{\bullet}$).[87,90−92]

Considering next the impact of an aqueous medium ($\varepsilon_s = 78.3$), a Mulliken analysis of spin density carried out for the reoptimized TS structure reveals no change in the net spin populations on the two fragments in solution, though an analysis of the total charge separation across the two fragments suggests a substantially more polarized transition state. In the gas phase, the fatty acid peroxyl radical is computed to have a charge that is ~0.08 electrons more negative than the tyrosine. In this treatment, neither fragment includes the proton in flight.

In the aqueous medium, the difference between the two fragments increases to 0.21 electrons. As a result, the solvated TS for concerted PCET has substantially more net charge transfer, even though the spin population is relatively unchanged. This effect is depicted in Figure 8, where the electrostatic potential of the two TS structures is visualized using a common color-mapping scale. Substantially greater polarity is evident in the solvated case.

Noting the comparisons above in relation to the computed ^{18}O KIEs, it is apparent that reactions in the high dielectric medium are more advanced along the electron transfer coordinate than the proton transfer coordinate, leading to normal as opposed to inverse isotope effects. It should be further noted that, in an enzyme, polarity derives more from the proximity of charged residues than from a bulk dielectric effect.[93] That is, the variation in this study of a homogeneous dielectric constant from 1 to ~80 simply provides a convenient way to probe the degree to which proton and electron transfer are subject to decoupling in the reactive configuration—in an enzyme with optimally positioned charged residues, larger electric fields than those induced through the solvent dielectric response are possible.[88,93] Therefore, the

dx.doi.org/10.1021/bi201016h | *Biochemistry* 2011, 50, 7375−7389

Figure 8. Electrostatic potential for a positive test charge ranging from repulsive (blue) to attractive (red) for the gas-phase (left) and aqueous (right) TS structures for concerted PCET. The same color scale is used for both structures, plotted on the 0.075 au isodensity surface, with the tyrosyl ring to the left and the methylbutanoate fragment to the right.

analysis here is directed to the general question of the role charge separation, due to proton and electron transfer, may play in determining heavy atom isotope effects.

The computational results support the assignment of the first irreversible step as concerted PCET in an aqueous continuum with a TS characterized by greater progress along the electronic coordinate than the protonic coordinate. Although enforced separation of the peroxyl radical and reduced tyrosine/tyrosinate could lead to more normal ^{18}O KIEs in a lower dielectric environment, this comes at the expense of an increased activation barrier along the Born−Oppenheimer surface, making it more difficult to explain the transfer of a hydrogen atom.

Although a sequential PCET mechanism where the electron transfers rapidly and reversibly prior to the proton cannot be rigorously excluded,[87] such a reaction would require the existence of a large stabilizing influence due to hydrogen bonding or electrostatics.[93] The details of such effects have been predicted theoretically but remain difficult to verify experimentally within enzyme active sites.[43,44] Importantly, experiments performed in this study over a range from neutral to basic pH/pDs provide no indication of electrostatic influences or prototropic equilibria.

CONCLUSIONS

The molecular oxygen reactivity of a tyrosyl radical-utilizing fatty acid α-dioxygenase has been experimentally and computationally examined under physiologically relevant conditions. The second-order rate constant, $k_{cat}/K_M(O_2)$, reflecting all steps beginning as O_2 enters the catalytic cycle, up to and including the first irreversible step, exhibits normal oxygen-18 kinetic isotope effects and a pH/pD-independent normal primary deuterium kinetic isotope effects. The latter arise from retention of the α-hydrogen atom abstracted from the fatty acid substrate. This observation, requiring slow solvent isotope exchange, corroborates earlier findings that hydrogen isotope scrambling from the solvent into the α-position of the fatty acid is inhibited by O_2.

The results rule out certain sequential proton-coupled electron transfer mechanisms for tyrosine oxidation by a substrate-derived peroxyl radical intermediate. Reversible proton transfer followed by electron transfer, as well as initial proton or electron transfer in the rate-limiting step are inconsistent with the observed deuterium and ^{18}O kinetic isotope effects. Reversible electron transfer prior to rate-limiting proton transfer is not rigorously excluded by the isotope effects, yet this alternative is difficult to reconcile with the pH/pD-insensitive kinetics and the ground state thermodynamics. In the absence of hydrogen bonding or electrostatic stabilization, the tyrosyl radical cation and fatty acid peroxide-containing intermediate lies >15 kcal mol^{-1} higher in energy than the separated reactants. Concerted proton-coupled electron transfer is, therefore, proposed to predominate in experiments performed at variable solution pH. This reaction is close to thermoneutral (ΔG° = 0 kcal mol^{-1}) on the basis of the similar tyrosine and hydroperoxide O−H bond strengths, consistent with the observed $\Delta G^{\ddagger}$ = 7.5 kcal mol^{-1} derived from the $k_{cat}/K_M(O_2)$.

This study has shown that concerted proton-coupled electron transfer from the reduced tyrosine cofactor to the α-peroxyl intermediate likely controls the selective formation of 2-(*R*)-hydroperoxide products in RαO at physiological O_2 concentrations. Importantly, the oxygen kinetic isotope effects are reproduced by analysis of the vibrational frequencies of the DFT-derived transition state in an aqueous medium, which is polarized such that there is greater progress along the coordinate for electron transfer than the coordinate for proton transfer. These findings illustrate the utility of density functional calculations and natural abundance oxygen-18 isotope effects in probing reactivity patterns of O_2 as well as identifying mechanisms of proton-coupled electron transfer.

ASSOCIATED CONTENT

Supporting Information

Additional experimental and computational details. This material is available free of charge via the Internet at http://pubs.acs.org.

AUTHOR INFORMATION

Corresponding Author

*E-mail jproth@jhu.edu, Tel (410) 516-7835, Fax(410) 516-8420 (J.P.R.). E-mail cramer@umn.edu, Tel (612) 624-0859, Fax (612) 626-7541 (C.J.C.).

Funding

J.P.R. and C.J.C. acknowledge support from the National Science Foundation grants MCB0919898 and CHE-0952054 as well as Department of Energy grant DE-FG02-09ER16094.

ABBREVIATIONS

RαO, rice fatty acid α-(di)oxygenase; PIOX, pathogen-inducible oxygenase; Por, protoporphyrin IX; EPR, electron paramagnetic resonance; FA, fatty acid; KIE, kinetic isotope effect; wt, wild-type; IRMS, isotope ratio mass spectrometry; DFT, density functional theory; GGA, generalized-gradient approximation; ZPE, zero point energy; EXC, excitation energy; MMI, mass moments of inertia; TST, transition state

theory; EIE, equilibrium isotope effect; PCET, proton-coupled electron transfer.

■ ADDITIONAL NOTES

[a]Data are provided in the Supporting Information of ref 17. [b]Calculations performed with Gaussian 09 and Gaussian03 are described in greater detail in the Supporting Information. [c]See the Supporting Information for details. [d]Assuming a pre-exponential factor of 10^{11} M^{-1} s^{-1} as suggested in ref 88.

■ REFERENCES

(1) Koeduka, T., Matsui, K., Akakabe, Y., and Kajiwara, T. (2002) Catalytic properties of rice α−oxygenase: a comparison with mammalian prostaglandin H synthases. *J. Biol. Chem. 277*, 22648−22655.

(2) Hamberg, M., Sanz, A., and Castresana, C. (1999) α-oxidation of fatty acids in higher plants. Identification of a pathogen-inducible oxygenase (PIOX) as an α-dioxygenase and biosynthesis of 2-hydroperoxylinolenic acid. *J. Biol. Chem. 274*, 24503−24513.

(3) Liu, W., Rogge, C. E., Bambai, B., Palmer, G., Tsai, A.-L., and Kulmacz, R. J. (2004) Characterization of the Heme Environment in Arabidopsis thaliana Fatty Acid α -Dioxygenase-1. *J. Biol. Chem. 279*, 29805−29815.

(4) Lee, D.-S., Nioche, P., Hamberg, M., and Raman, C. S. (2008) Structural insights into the evolutionary paths of oxylipin biosynthetic enzymes. *Nature 455*, 363−368.

(5) Andreou, A., Brodhun, F., and Feussner, I. (2009) Biosynthesis of oxylipins in non-mammals. *Prog. Lipid Res. 48*, 148−170.

(6) Tang, D. G., La, E., Kern, J., and Kehrer, J. P. (2002) Fatty acid oxidation and signaling in apoptosis. *Biol. Chem. 383*, 425−442.

(7) Koeduka, T., Matsui, K., Hasegawa, M., Akakabe, Y., and Kajiwara, T. (2005) Rice fatty acid α -dioxygenase is induced by pathogen attack and heavy metal stress: Activation through jasmonate signaling. *J. Plant Physiol. 162*, 912−920.

(8) Meisner, A. K., Saffert, A., Schreier, P., and Schoen, A. (2009) Fatty acid α−dioxygenase from Pisum sativum: temporal and spatial regulation during germination and plant development. *J. Plant Physiol. 166*, 333−343.

(9) Hamberg, M., Sanz, A., Rodriguez, M. J., Calvo, A. P., and Castresana, C. (2003) Activation of the fatty acid α -dioxygenase pathway during bacterial infection of tobacco leaves: formation of oxylipins protecting against cell death. *J. Biol. Chem. 278*, 51796−51805.

(10) Cardinale, F., Fammartino, A., Tamietti, G., Feussner, I., and Esquerre-Tugaye, M.-T. (2010) Oxylipins and relevant enzymes in plant defence, *Adv. Plant Physiol. 11*, 215−225.

(11) Brodhun, F., and Feussner, I. (2011) Oxylipins in fungi. *FEBS J. 278*, 1047−1063.

(12) Hoffmann, I., Jerneren, F., Garscha, U., and Oliw, E. H. (2011) Expression of 5,8-LDS of Aspergillus fumigatus and its dioxygenase domain. A comparison with 7,8-LDS, 10-dioxygenase, and cyclooxygenase. *Arch. Biochem. Biophys. 506*, 216−222.

(13) Garscha, U., Jerneren, F., Chung, D., Keller, N. P., Hamberg, M., and Oliw, E. H. (2007) Identification of Dioxygenases Required for Aspergillus Development: Studies of Products, Stereochemistry, and the Reaction Mechanism. *J. Biol. Chem. 282*, 34707−34718.

(14) Garscha, U., and Oliw, E. H. (2009) Leucine/Valine Residues Direct Oxygenation of Linoleic Acid by (10R)- and (8R)-Dioxygenases: expression and site-directed mutagenesis of (10R)-dioxygenase with epoxyalcohol synthase activity. *J. Biol. Chem. 284*, 13755−13765.

(15) Rouzer, C. A., and Marnett, L. J. (2003) Mechanism of Free Radical Oxygenation of Polyunsaturated Fatty Acids by Cyclooxygenases. *Chem. Rev. 103*, 2239−2304.

(16) Tsai, A.-L., and Kulmacz, R. J. (2010) Prostaglandin H synthase: Resolved and unresolved mechanistic issues. *Arch. Biochem. Biophys. 493*, 103−124.

(17) Gupta, A., Mukherjee, A., Matsui, K., and Roth, J. P. (2008) Evidence for Protein Radical-Mediated Nuclear Tunneling in Fatty Acid α-Oxygenase. *J. Am. Chem. Soc. 130*, 11274−11275.

(18) Mukherjee, A., Angeles-Boza, A. M., Huff, G. S., and Roth, J. P. (2011) Catalytic Mechanism of a Heme and Tyrosyl Radical-Containing Fatty Acid α-(Di)oxygenase. *J. Am. Chem. Soc. 133*, 227−238.

(19) Lloyd, T., Krol, A., Campanaro, D., and Malkowski, M. (2006) Purification, crystallization and preliminary X-ray diffraction analysis of pathogen-inducible oxygenase (PIOX) from Oryza sativa. *Acta Crystallogr., Sect. F F62*, 365−367.

(20) Koszelak-Rosenblum, M., Krol, A. C., Simmons, D. M., Goulah, C. C., Wroblewski, L., and Malkowski, M. G. (2008) His-311 and Arg-559 Are Key Residues Involved in Fatty Acid Oxygenation in Pathogen-inducible Oxygenase. *J. Biol. Chem. 283*, 24962−24971.

(21) Hays, A.-M. A., Vassiliev, I. R., Golbeck, J. H., and Debus, R. J. (1998) Role of D1-His190 in proton-coupled electron transfer reactions in photosystem II: A chemical complementation study. *Biochemistry 37*, 11352−11365.

(22) Faller, P., Goussias, C., Rutherford, A. W., and Un, S. (2003) Resolving intermediates in biological proton-coupled electron transfer: A tyrosyl radical prior to proton movement. *Proc. Natl. Acad. Sci. U. S. A. 100*, 8732−8735.

(23) Hatcher, E., Soudackov, A. V., and Hammes-Schiffer, S. (2004) Proton-Coupled Electron Transfer in Soybean Lipoxygenase. *J. Am. Chem. Soc. 126*, 5763−5775.

(24) Dunford, H. B. (1999) *Heme Peroxidases*, Wiley, New York.

(25) Saffert, A., Hartmann-Schreier, J., Schon, A., and Schreier, P. A. (2000) A dual function α-dioxygenase-peroxidase and NAD+ oxidoreductase active enzyme from germinating pea rationalizing α-oxidation of fatty acids in plants. *Plant Physiol. 123*, 1545−1551.

(26) Halliwell, B., and Gutteridge, J. M. C. (1999) *Free Radicals In Biology and Medicine*, 3rd ed., pp 1−22, Oxford University Press, London.

(27) Valentine, J. S., Foote, C. S., Greenberg, A., and Liebman, J. F. (1995) *Active Oxygen in Biochemistry*, pp 276−312, Chapman & Hall, London.

(28) Schramm, V.L. (2007) Enzymatic Transition State Theory and transition state design. *J. Biol. Chem. 282*, 28297−28300.

(29) Berry, E. A., and Trumpower, B. L. (1987) Simultaneous determinations of hemes a, b, and c from pyridine hemochrome spectra. *Anal. Biochem. 161*, 1−15.

(30) Cornish-Bowden, A. (1995) *Fundamentals of Enzyme Kinetics*, 2nd ed., Portland Press, London.

(31) Brouwer, A.C., and Kirsch, J. F. (1982) Investigation of diffusion-limited rates of chymotrypsin reactions by viscosity variation. *Biochemistry 21*, 1302−1307.

(32) Nakatani, H., and Dunford, H. B. (1979) Meaning of diffusion-controlled association rate constants in enzymology. *J. Phys. Chem. 83*, 2662−2665.

(33) Hasinoff, B. B., and Chishti, S. B. (1982) Viscosity dependence of the kinetics of the diffusion-controlled reaction of carbon monoxide and myoglobin. *Biochemistry 21*, 4275−4278.

(34) Dunford, H. B., and Hasinoff, B. B. (1986) On the rates of enzymic, protein and model compound reactions: the importance of diffusion control. *J. Inorg. Biochem. 28*, 263−269.

(35) Glasoe, P. K., and Long, F. A. (1960) Use of glass electrodes to measure acidities in deuterium oxide. *J. Phys. Chem. 64*, 188−190.

(36) Smirnov, V. V., Brinkley, D. W., Lanci, M. P., Karlin, K. D., and Roth, J. P. (2006) Probing metal-mediated O_2 activation in chemical and biological systems. *J. Mol. Catal. A: Chem 251*, 100−107.

(37) Guy, R. D., Fogel, M. L., and Berry, J. A. (1993) Photosynthetic fractionation of the stable isotopes of oxygen and carbon. *Plant Physiol. 101*, 37−47.

(38) Cramer, C. J. (2004) *Essentials of Computational Chemistry: Theories and Models*, 2nd ed., Wiley, Chichester, England.

(39) Perdew, J. P., and Wang, Y. (1986) Accurate and Simple Density Functional for the Electronic Exchange Energy: Generalized Gradient Approximation. *Phys. Rev. B 33*, 8800−8802.

(40) Perdew, J. P. (1991) Unified Theory of Exchange and Correlation Beyond the Local Density Approximation, in *Electronic Structure of Solids '91* (Ziesche, P., and Eschrig, H., Eds.) pp 11−20, Akademie Verlag, Berlin.

(41) Adamo, C., and Barone, V. (1998) Exchange functionals with improved long-range behavior and adiabatic connection methods without adjustable parameters: The *m*PW and *m*PW1PW Models. *J. Chem. Phys. 108*, 664−675.

(42) Hehre, W. J., Radom, L., Schleyer, P. V., and Pople, J. A. (1986) *Ab Initio Molecular Orbital Theory*, Wiley, New York.

(43) Roth, J. P., Wincek, R., Nodet, G., Edmondson, D. E., McIntire, W. S., and Klinman, J. P. (2004) Oxygen isotope effects on electron transfer to O_2 probed using chemically modified flavins bound to glucose oxidase. *J. Am. Chem. Soc. 126*, 15120−15131.

(44) Roth, J. P., and Klinman, J. P. (2003) Catalysis of electron transfer during activation of O_2 by the flavoprotein glucose oxidase. *Proc. Natl. Acad. Sci. U. S. A. 100*, 62−67.

(45) Cramer, C. J., and Truhlar, D. G. (1999) Implicit solvation models: equilibria, structure, spectra, and dynamics. *Chem. Rev. 99*, 2161−2200.

(46) Tomasi, J., Mennucci, B., and Cammi, R. (2005) Quantum Mechanical Continuum Solvation Models. *Chem. Rev. 105*, 2999−3093.

(47) Marenich, A. V., Cramer, C. J., and Truhlar, D. G. (2009) Universal Solvation Model Based on Solute Electron Density and on a Continuum Model of the Solvent Defined by the Bulk Dielectric Constant and Atomic Surface Tensions. *J. Phys. Chem. B 113*, 6378−6396.

(48) Cramer, C. J., and Truhlar, D. G. (2008) A Universal Approach to Solvation Modeling. *Acc. Chem. Res. 41*, 760−768.

(49) Cramer, C. J., and Truhlar, D. G. (2009) Reply to Comment on "A Universal Approach to Solvation Modeling. *Acc. Chem. Res. 42*, 493−497.

(50) Warshel, A., Sharma, P. K., Kato, M., and Parson, W. W. (2006) Modeling electrostatic effects in proteins. *Biochim. Biophys. Acta, Proteins Proteomics 1764*, 1647−1676.

(51) Bigeleisen, J., and Mayer, M. G. (1947) Calculation of equilibrium constants for isotopic exchange reactions. *J. Chem. Phys. 15*, 261−267.

(52) Ashley, D.C., Brinkley, D. W., and Roth, J. P. (2010) Oxygen isotope effects as structural and mechanistic probes in inorganic oxidation chemistry. *Inorg. Chem. 49*, 3661−3675.

(53) Roth, J. P. (2009) Oxygen isotope effects as probes of electron transfer mechanisms and structures of activated O_2. *Acc. Chem. Res. 42*, 399−408.

(54) Liu, Q., Tossell, J. A., and Liu, Y. (2010) On the proper use of the Bigeleisen - Mayer equation and corrections to it in the calculation of isotopic fractionation equilibrium constants. *Geochim. Cosmochim. Acta 74*, 6965−6983.

(55) Smirnov, V. V., Lanci, M. P., and Roth, J. P. (2009) Computational modeling of oxygen isotope effects on metal-mediated O_2 activation at varying temperatures. *J. Phys. Chem. A 113*, 1934−1945, and references therein.

(56) Cape, J. L., Bowman, M. K., and Kramer, D. M. (2005) Reaction intermediates of quinol oxidation in a photoactivatable system that mimics electron transfer in the cytochrome bc1 complex. *J. Am. Chem. Soc. 127*, 4208−4215.

(57) Ludlow, M.K., Soudackov, A. V., and Hammes-Schiffer, S. (2009) Theoretical analysis of the unusual temperature dependence of the kinetic isotope effect in quinol oxidation. *J. Am. Chem. Soc. 131*, 7094−7102.

(58) Kim, S. F., Huri, D. A., and Snyder, S. H. (2005) Inducible nitric oxide synthase binds, S-nitrosylates, and activates cyclooxygenase-2. *Science 310*, 1966−1970.

(59) Mirica, L. M., McCusker, K. P., Munos, J. W., Liu, H., and Klinman, J. P. (2008) ^{18}O kinetic isotope effects in non-heme iron enzymes: probing the nature of Fe/O_2 Intermediates. *J. Am. Chem. Soc. 130*, 8122−8123.

(60) Klinman, J. P., Berry, J. A., and Tian, G. (1993) in *Bioinorganic Chemistry of Copper* (Karlin, K. D., and Tyeklar, Z., Eds.), p 151, Chapman & Hall, New York.

(61) Klinman, J. P. (2001) Life as aerobes: are there simple rules for activation of dioxygen by enzymes? *J. Biol. Inorg. Chem. 6*, 1−13.

(62) Roth, J. P., and Klinman, J. P. (2006) Oxygen-18 isotope effects as a probe of enzymatic activation of molecular oxygen, in *Isotope Effects in Chemistry and Biology* (Kohen, A., Limbach, H.-H., Eds.) pp 645−669, CRC Press, Boca Raton, FL.

(63) Hirschi, J., and Singleton, D. A. (2005) The Normal Range for Secondary Swain-Schaad Exponents without Tunneling or Kinetic Complexity. *J. Am. Chem. Soc. 127*, 3294−3295.

(64) Meyer, M. P., and Klinman, J. P. (2011) Investigating inner-sphere reorganization via secondary kinetic isotope effects in the C-H cleavage reaction catalyzed by soybean lipoxygenase: tunneling in the substrate backbone as well as the transferred hydrogen. *J. Am. Chem. Soc. 133*, 430−439, and references therein.

(65) Lanci, M. P., Brinkley, D. W., Stone, K. L., Smirnov, V. V., and Roth, J. P. (2005) Structures of transition states in metal-mediated O_2-activation reactions. *Angew. Chem., Int. Ed. 44*, 7273−7276.

(66) Lanci, M. P., and Roth, J. P. (2006) Oxygen Isotope Effects upon Reversible O_2-Binding Reactions: Characterizing Mononuclear Superoxide and Peroxide Structures. *J. Am. Chem. Soc. 128*, 16006−16007.

(67) Roth, J. P., and Cramer, C. J. (2008) Direct Examination of H_2O_2 Activation by a Heme Peroxidase. *J. Am. Chem. Soc. 130*, 7802−7803.

(68) Mukherjee, A., Smirnov, V. V., Lanci, M. P., Brown, D. E., Shepard, E. M., Dooley, D. M., and Roth, J. P. (2008) Inner-sphere mechanism for molecular oxygen reduction catalyzed by copper amine oxidases. *J. Am. Chem. Soc. 130*, 9459−9473.

(69) Humphreys, K. J., Mirica, L. M., Wang, Y., and Klinman, J. P. (2009) Galactose oxidase as a model for reactivity at a copper superoxide center. *J. Am. Chem. Soc. 131*, 4657−4663.

(70) Smith, W. L., DeWitt, D. L., and Garavito, R. M. (2000) Cyclooxygenases: structural, cellular, and molecular biology. *Annu. Rev. Biochem. 69*, 145−182.

(71) Thuresson, E. D., Lakkides, K. M., Rieke, C. J., Sun, Y., Wingerd, B. A., Micielli, R., Mulichak, A. M., Malkowski, M. G., Garavito, R. M., and Smith, W. L. (2001) Prostaglandin endoperoxide H synthase-1. The functions of cyclooxygenase active site residues in the binding, positioning, and oxygenation of arachidonic acid. *J. Biol. Chem. 276*, 10347−10358.

(72) Wecksler, A. T., Kenyon, V., Garcia, N. K., Deschamps, J. D., van der Donk, W. A., and Holman, T. R. (2009) Kinetic and Structural Investigations of the Allosteric Site in Human Epithelial 15-Lipoxygenase-2. *Biochemistry 48*, 8721−8730.

(73) Wecksler, A. T., Jacquot, C., van der Donk, W. A., and Holman, T. R. (2009) Mechanistic Investigations of Human Reticulocyte 15- and Platelet 12-Lipoxygenases with Arachidonic Acid. *Biochemistry 48*, 6259−6267.

(74) Furse, K. E., Pratt, D. A., Schneider, C., Brash, A. R., Porter, N. A., and Lybrand, T. P. (2006) Molecular Dynamics Simulations of Arachidonic Acid-Derived Pentadienyl Radical Intermediate

Complexes with COX-1 and COX-2: Insights into Oxygenation Regio- and Stereoselectivity. *Biochemistry 45*, 3206−3218.

(75) Glickman, M. H., Cliff, S., Thiemens, M., and Klinman, J. P. (1997) Comparative study of ^{17}O and ^{18}O isotope effects as a probe for dioxygen activation: Application to the soybean lipoxygenase reaction. *J. Am. Chem. Soc. 119*, 11357−11361.

(76) Knapp, M. J., and Klinman, J. P. (2003) Kinetic studies of oxygen reactivity in soybean lipoxygenase-1. *Biochemistry 42*, 11466−11475.

(77) Mukherjee, A., Brinkley, D. W., Chang, K.-M., and Roth, J. P. (2007) Molecular oxygen dependent steps in fatty acid oxidation by cyclooxygenase-1. *Biochemistry 46*, 3975−3989.

(78) Hermes, J.D., Roeske, C. A., O'Leary, M. H., and Cleland, W. W. (1982) Use of multiple isotope effects to determine enzyme mechanisms and intrinsic isotope effects. Malic enzyme and glucose 6-phosphate dehydrogenase. *Biochemistry 21*, 5106−5114.

(79) Cook, P. F., and Cleland, W. W. (2007) *Enzyme Kinetics and Mechanism*, pp 277−280, Garland Science, New York.

(80) Tian, G. (1992) Effective rate constants and general isotope effect equations for steady state enzymic reactions with multiple isotope-sensitive steps. *Bioorg. Chem. 20*, 95−106.

(81) Tian, G., Berry, J. A., and Klinman, J. P. (1994) Oxygen-18 kinetic isotope effects in the dopamine β -monooxygenase reaction: Evidence for a new chemical mechanism in non-heme, metallomonooxygenase. *Biochemistry 33*, 226−234.

(82) Hermes, J. D., Weiss, P. M., and Cleland, W. W. (1985) Use of nitrogen-15 and deuterium isotope effects to determine the chemical mechanism of phenylalanine ammonia-lyase. *Biochemistry 24*, 2959−2967.

(83) Brinkley, D. W., and Roth, J. P. (2005) Determination of a Large Reorganization Energy Barrier for Hydride Abstraction by Glucose Oxidase. *J. Am. Chem. Soc. 127*, 15720−15721.

(84) Roth, J. P., Lovell, S., and Mayer, J. M. (2000) Intrinsic Barriers for Electron and Hydrogen Atom Transfer Reactions of Biomimetic Iron Complexes. *J. Am. Chem. Soc. 122*, 5486−5498.

(85) Khaikin, G. I., Alfassi, Z. B., Huie, R. E., and Neta, P. (1996) Oxidation of Ferrous and Ferrocyanide Ions by Peroxyl Radicals. *J. Phys. Chem. 100*, 7072−7077.

(86) Dixon, W. T., and Murphy, D. (1976) Determination of the acidity constants of some phenol radical cations by means of electron spin resonance. *J. Chem. Soc., Faraday Trans. 272*, 1221−1230.

(87) Litwinienko, G., and Ingold, K. U. (2007) Solvent Effects on the Rates and Mechanisms of Reaction of Phenols with Free Radicals. *Acc. Chem. Res. 40*, 222−230.

(88) Marcus, R. A., and Sutin, N. (1985) Electron transfers in chemistry and biology. *Biochim. Biophys. Acta, Rev. Bioenerg. 811*, 265−322.

(89) Warren, J. J., Tronic, T. A., and Mayer, J. M. (2010) Thermochemistry of proton-coupled electron transfer reagents and its implications. *Chem. Rev. 110*, 6961−7001.

(90) Lingwood, M., Hammond, J. R., Hrovat, D. A., Mayer, J. M., and Borden, W. T. (2006) MPW1K performs much better than B3LYP in DFT calculations on reactions that proceed by proton-coupled electron transfer (PCET). *J. Chem. Theory Comput. 2*, 740−745.

(91) Isborn, C., Hrovat, D. A., Borden, W. T., Mayer, J. M., and Carpenter, B. K. (2005) Factors controlling the barriers to degenerate hydrogen atom transfers. *J. Am. Chem. Soc. 127*, 5794−5795.

(92) Skone, J. H., Soudackov, A. V., and Hammes-Schiffer, S. (2006) Calculation of vibronic couplings for phenoxyl/phenol and benzyl/toluene self-exchange reactions: implications for proton-coupled electron transfer mechanisms. *J. Am. Chem. Soc. 128*, 16655−16663.

(93) Warshel, A., Sharma, P. K., Kato, M., Xiang, Y., Liu, H., and Olsson, M. H. M. (2006) Electrostatic basis for enzyme catalysis. *Chem. Rev. 106*, 3210−3235.